J|A|C|S
ARTICLES
Published on Web 09/18/2004

Aromatic Gold and Silver 'Rings': Hydrosilver(I) and Hydrogold(I) Analogues of Aromatic Hydrocarbons

Constantinos A. Tsipis,*,† Eustathios E. Karagiannis,† Panagiota F. Kladou,† and Athanassios C. Tsipis‡

Laboratory of Applied Quantum Chemistry, Faculty of Chemistry, Aristotle University of Thessaloniki, 541 24 Thessaloniki, Greece, and Laboratory of Inorganic and General Chemistry, Department of Chemistry, University of Ioannnina, Ioannina 451 10, Greece

Received May 25, 2004; E-mail: tsipis@chem.auth.gr

Abstract: Quantum chemical calculations suggest that a series of molecules with the general formula *cyclo*-$M_n(\mu\text{-H})_n$ (M = Ag, Au; $n = 3-6$) are stable. All *cyclo*-M_nH_n species, except *cyclo*-Au_3H_3, have the same symmetry with the respective aromatic hydrocarbons but differ in that the hydrogen atoms are in bridging positions between the metal atoms and not in terminal positions. The aromaticity of the hydrosilver(I) and hydrogold(I) analogues of aromatic hydrocarbons was verified by a number of established criteria of aromaticity, such as structural, energetic, magnetic, and chemical criteria. In particular, the nucleus-independent chemical shift, the relative hardness, $\Delta\eta$, the electrophilicity index, ω, and the chemical reactivity toward electrophiles are indicative for the aromaticity of the hydrosilvers(I) and hydrogolds(I). A comprehensive study of the structural, energetic, spectroscopic (IR, NMR, electronic, and photoelectron spectra), and bonding properties of the novel classes of inorganic compounds containing bonds that are characterized by a common ring-shaped electron density, more commonly seen in organic molecules, is presented.

Introduction

Recently, we have communicated on a new class of cyclic copper(I) hydrides (hydrocoppers) formulated as Cu_nH_n ($n = 3-6$) as the cyclic hydrocarbon analogues in the diverse tapestry of inorganic chemistry.[1] The choice of the copper(I) hydrides was based on the well-known tendency of copper(I) centers to cluster together in a variety of organocopper(I) compounds[2−12] involving even the alkyl groups as bridging ligands, a representative example being the cyclic Cu_4R_4 tetramer.[13] The cyclic hydrocoppers(I) and some of their substituted derivatives were predicted to be stable species with a perfectly planar configuration, thus expanding the borders of inorganic chemistry into the realm of organic chemistry by building molecules containing bonds that are characterized by a common ring-shaped electron density, more commonly seen in organic molecules, with new properties and chemical reactivity. Moreover, these findings may not only expand the aromaticity concept in all-metal systems with structures resembling those of the aromatic hydrocarbons but may also indicate whole classes of new inorganic aromatic species (substituted derivatives), resulting upon substitution of the H atoms by other groups such as alkyls (R) and aryls (Ar), halides (X), amido (NR_2), hydroxide (OH) and alkoxides (OR), etc. Considering that the two other coinage metals, e.g., Ag(I) and Au(I), also exhibit a strong tendency to cluster together in a variety of organosilver(I)[14−27] and organogold(I)[28−51] com-

† Aristotle University of Thessaloniki.
‡ University of Ioannina.

(1) Tsipis, A. C.; Tsipis, C. A. *J. Am. Chem. Soc.* **2003**, *125*, 1136.
(2) Vega, A.; Calvo, V.; Spodine, E.; Zarate, A.; Fuenzalida V.; Sailard, J.-Y. *Inorg. Chem.* **2002**, *41*, 532.
(3) Yam, V. W.-W.; Fung, W. K.-M.; Cheung, K.-K. *J. Cluster Sci.* **1999**, *10*, 37.
(4) Yam, V. W.-W.; Fung, W. K.-M.; Cheung, K.-K. *Organometallics* **1998**, *17*, 3293.
(5) Niemeyer, M. *Organometallics* **1998**, *17*, 4649 and references therein.
(6) Hermann, E.; Richter, R.; Chau, N. *Z. Anorg. Allg. Chem.* **1997**, *623*, 403.
(7) Eriksson, H.; Håkansson, M. *Organometallics* **1997**, *16*, 4243.
(8) Eriksson, H.; Örtendhal, M.; Håkansson, M. *Organometallics* **1996**, *15*, 4823.
(9) Yam, V. W.-W.; Lee, W.-K.; Lai, T.-F. *Organometallics* **1993**, *12*, 2383.
(10) Knotter, D. M.; Grove, D. M.; Smeets, W. J.; Spek, A. L.; van Koten, G. *J. Am. Chem. Soc.* **1992**, *114*, 3400.
(11) Olmstead, M. M.; Power, P. P. *J. Am. Chem. Soc.* **1990**, *112*, 8008.
(12) Meyer, E. M.; Gambarotta, S.; Florlani, C.; Chiesi-Villa, A.; Guastini, C. *Organometallics* **1989**, *8*, 1067.
(13) Jarvis, J. A. J.; Kilbourn, B. T.; Pearce, R.; Lappert, M. F. *J. Chem. Soc., Chem. Commun.*, **1973**, 475.
(14) Yam, V. W.-W.; Lo, K. K.-Y. *Chem. Soc. Rev.* **1999**, *28*, 323.
(15) Tse, M. C.; Che, C. M.; Miskowski, V. M. *J. Am. Chem. Soc.* **1999**, *121*, 4799.
(16) Zhu, H.-L.; Zhang, X.-M.; Liu, X.-Y.; Liu, G.-F.; Usman, A.; Fun, H.-K. *Inorg. Chem. Commun.* **2003**, *6*, 1113.
(17) Rawashdeh-Omary, M. A.; Omary, M. A.; Patterson, H. H. *J. Am. Chem. Soc.* **2000**, *122*, 10371.
(18) Codina, A.; Fernández, E. J.; Jones, P. G.; Laguna, A.; López-de-Luzuriaga, J. M.; Monge, M.; Olmos, M. E.; Pérez, J.; Rodriguez, M. A. *J. Am. Chem. Soc.* **2002**, *124*, 6781.
(19) Catalano, V. J.; Malwitz, M. A. *Inorg. Chem.* **2003**, *42*, 5483.
(20) Fernández, E. J.; López-de-Luzuriaga, J. M.; Monge, M.; Olmos, M. E.; Pérez, J.; Laguna, A.; Mohamed, A. A.; Fackler, J. P., Jr. *J. Am. Chem. Soc.* **2003**, *125*, 2022.
(21) Janata, E. *J. Phys. Chem. B* **2003**, *107*, 7334.
(22) Garrison, J. C.; Simons, R. S.; Tessier, C. A.; Youngs, W. J. *J. Organomet. Chem.* **2003**, *673*, 1.
(23) Eisler, D. J.; Kirby, C. W.; Puddephatt, R. J. *Inorg. Chem.* **2003**, *42*, 7626.
(24) Tsyba, I.; Mui, B. B.; Bau, R.; Noguchi, R.; Nomiya, K. *Inorg. Chem.* **2003**, *42*, 8028.
(25) Meyer, E. M.; Gambarotta, S.; Floriani, C.; Chiesi-Villa, A.; Guastini, C. *Organometallics* **1989**, *8*, 1067.
(26) Albano, V. G.; Azzaroni, F.; Iapalucci, M. C.; Longoni, G.; Morani, M.; Mulley, S.; Proserpio, D. M.; Sironi, A. *Inorg. Chem.* **1994**, *33*, 5320.
(27) Eisler, D. J.; Kirby, C. W.; Puddephatt, R. J. *Inorg. Chem.* **2003**, *42*, 7626.

10.1021/ja0469277 CCC: $27.50

pounds formulated as M_nL_n (M = Ag or Au; L = a variety of bridging ligands), we thought it would be advisable to extend our studies to hydrosilver(I) and hydrogold(I) analogues of aromatic hydrocarbons and explore the factors responsible for their perfect planarity and high stability. In particular, the attractive $d^{10}-d^{10}$ interactions between closed-shell copper(I), silver(I), or gold(I) centers seem to be important in determining the structures of many copper(I), silver(I), and gold(I) complexes. The most typical case is found in gold(I) chemistry, where the term *aurophilicity*, coined by Schmidbaur,[52,53] was used to describe these relatively weak metal−metal interactions. The modern advances in the science of gold have recently been reviewed in a comprehensive monograph by Schmidbaur.[33] Noteworthy is the comparable strength of aurophilicity to that of the hydrogen bonding (ca. 7−11 kcal/mol), which was attributed to the combination of correlation and relativistic effects.[54−56] Similarly, the terms cuprophilicity and argentophilicity have been used to describe the weakly bonding d^{10} interactions which support the self-association of the copper(I), silver(I), and gold(I) complexes to form three-, four-, five-, and six-membered metal rings and other extended chains. It should be stressed that all metallic rings studied herein were found in a variety of silver(I)[14−27] and gold(I)[28−51] polynuclear complexes studied so far. Therefore, it would be important to survey briefly the structural features of the most representative examples of the three-, four-, five-, and six-membered silver(I) and gold(I) rings studied experimentally. Thus, the silver(I) triangle exhibiting short Ag−Ag bond distances of 272.5, 276.9, and 277.2 pm has very recently been found in the homoleptic carbene-bridged $[(\mu\text{-NHC})_3Ag_3]^{3+}$ species.[19] Similarly, the four-membered $[Ag_4]^{4+}$ planar parallelogram with Ag−Ag bond distances of 285.1 pm has very recently been found in the homoleptic carbene-bridged $[(\mu\text{-NHC})_4Ag_4]^{4+}$ species.[22] An almost perfect Ag_4 square was found several years ago[25] in the $[(\mu\text{-Mes})_4Ag_4]$ (Mes = 2,4,6-$Me_3C_6H_2$) complex; the Ag−Ag separation distances were 273.3 and 275.5 pm, while the Ag−Ag−Ag bond angles are very close to 90.0°. An idealized square of silver atoms (average Ag−Ag bond distance = 314.9 pm) surrounded by four edge-bridging $Fe(CO)_4$ groups composes the core structure of the $[Ag_4\{\mu\text{-Fe}(CO)_4\}_4]^{4-}$ complex.[26] As far as we know, no cyclic planar pentasilver(I) complexes have been synthesized so far. In a very recent paper,[27] the $[P_4Ag_5X_5]$ [P = (diphenylphosphinito)resorcinarene ligand] halide crown-like clusters have been synthesized and their structures were determined by X-ray crystallography. However, the complexes are formed on the basis of $P_4Ag_4(\mu\text{-}I_4)$ units, and these incorporate a fifth halide ion at the center and a fifth Ag(I) ion at the top to give the final $P_4Ag_5X_5$ units. Cyclic planar hexanuclear silver(I) complexes are also very rare. The synthesis and structures of the hexanuclear silver(I) nicotinate clusters $[Ag(Hmna)_6]$ and $[Ag(mna)_6]^{6-}$ (mna = 2-mercaptonicotinate ligand) have recently been reported.[24] These clusters have an Ag_6S_6 core and an overall shape of a twisted hexagonal cylinder with six sulfur atoms and six silver atoms alternating on a puckered drumlike surface. The Ag−Ag separation distances were found to be in the range of 291.1−334.9 pm.

The chemistry of cyclic planar polynuclear complexes of gold(I), particularly those involving the four-membered ring, is more rich. Thus, the Au_3 triangle consists the core structure of carbeniate $[Au(\mu\text{-C,N}-R'N{=}COR)]_3$ (R = aryl or alkyl) and benzimidazolate $[Au(\mu\text{-}C^2,N^3\text{-bzim})]_3$ (bzim = 1-benzimidazolate) complexes.[31] These complexes are aurophilically bonded intramolecularly with Au···Au separation distances in the range of 331.2−337.1 pm, while several of them in the solid state are also aurophilically bonded intermolecularly with shorter Au···Au separation distances of 322.0−335.5 pm. Most important is the tendency of the Au_3-triangle-containing molecules to stack with a variety of organic and organometallic π acid molecules, such as the $[Hg(\mu\text{-C,C}-C_6F_4)]_3$ complex[39] and nitro-substituted fluorenones,[29] and interact with metal cations, such as Ag(I) and Tl(I), to form "sandwich" complexes analogous to metallocenes.[28] Interestingly, some of these complexes display the novel property of solvoluminescence.[29,31] The Au_3 triangle capped with O, N, or S donor atoms also composes the core structure in a series of complexes formulated as $[XAu_3]^+$ and $\{X[Au(PR_3)]_3\}^+$ (X = O, N, or S).[42,43] The aurophilic interactions in these complexes have exhaustively been investigated very recently[44] by quasi-relativistic DFT calculations. Aurophilic

(28) Burini, A.; Bravi, R.; Fackler, J. P., Jr.; Galassi, R.; Grant, T. A.; Omary, M. A.; Pietroni, B. R.; Staples, R. J. *Inorg. Chem.* **2000**, *39*, 3158.
(29) (a) Olmstead, M. M.; Jiang, F.; Attar, S.; Balch, A. L. *J. Am. Chem. Soc.* **2001**, *123*, 3260. (b) Balch, A. L.; Olmstead, M. M.; Vickery, J. C. *Inorg. Chem.* **1999**, *38*, 3494.
(30) Albano, V. G.; Castellari, C.; Femoni, C.; Iapalucci, M. C.; Longoni, G.; Monari, M.; Zacchini, S. *J. Cluster. Sci.* **2001**, *12*, 75.
(31) Fackler, J. P., Jr. *Inorg. Chem.* **2002**, *41*, 6959 and references therein.
(32) (a) Mohamed, A. A.; López-de-Luguriaga, J. M.; Fackler, J. P., Jr. *J. Cluster. Sci.* **2003**, *14*, 61. (b) Mohamed, A. A.; Abdou, H. E.; Irwin, M. D.; López-de-Luguriaga, J. M.; Fackler, J. P., Jr. *J. Cluster. Science.* **2003**, *14*, 253.
(33) Schmidbaur, H. *Gold: Chemistry, Biochemistry and Technology*; Wiley: Chichester, 1999.
(34) Yang, G.; Raptis, R. G. *Inorg. Chim. Acta* **2003**, *352*, 98.
(35) Mohamed, A. A.; Chen, J.; Bruce, A. E.; Bruce, M. R. M.; Bauer, J. A. K.; Hill, D. T. *Inorg. Chem.* **2003**, *42*, 2203.
(36) Bardaji, M.; Laguna, A. *Eur. J. Inorg. Chem.* **2003**, 3069 and references therein.
(37) White-Morris, R.; Stender, M.; Tinti, D. S.; Balch, A. L.; Rios, D.; Attar, S. *Inorg. Chem.* **2003**, *42*, 3237.
(38) Stefanescu, D. M.; Yuen, H. F.; Glueck, D. S.; Golen, J. A.; Zakharov, L. N.; Incarvito, C. D.; Rheingold, A. L. *Inorg. Chem.* **2003**, *42*, 8891.
(39) (a) Burini, A.; Fackler, J. P., Jr.; Galassi, R.; Grant, T. A.; Omary, M. A.; Rawashdeh-Omary, M. A.; Pietroni, B. R.; Staples, R. J. *J. Am. Chem. Soc.* **2000**, *122*, 11264. (b) Burini, A.; Fackler, J. P., Jr.; Galassi, R.; Macchioni, A.; Omary, M. A.; Rawashdeh-Omary, M. A.; Pietroni, B. R.; Sabatini, S.; Zuccaccia, C. *J. Am. Chem. Soc.* **2002**, *124*, 4570.
(40) Vickery, J. C.; Olmstead, M. M.; Fung, E. Y.; Balch, A. L. *Angew. Chem., Int. Ed. Engl.* **1997**, *36*, 1179.
(41) Rawashdeh-Omary, M. A.; Omary, M. A.; Fackler, J. P. *J. Am. Chem. Soc.* **2001**, *123*, 9689.
(42) (a) Angermaier, K.; Schmidbaur, H. *Chem. Ber.* **1994**, *127*, 2387. (b) Schmidbaur, H.; Kolb, A.; Zeller, E.; Schier, A.; Beruda, H. *Z. Anorg. Allg. Chem.* **1993**, *619*, 1575. (c) Angermaier, K.; Schmidbaur, H. *Acta Crystallogr. C* **1995**, *51*, 1793. (d) Angermaier, K.; Schmidbaur, H. *Inorg. Chem.* **1994**, *33*, 2069. (e) Schmidbaur, H.; Zeller, E.; Weidenhiller, G.; Steigelmann, O.; Beruda, H. *Inorg. Chem.* **1992**, *31*, 2370. (f) Schmidbaur, H.; Gabbai, F. P.; Schier, A.; Riede, J. *Organometallics* **1995**, *14*, 4969. (g) Bachman, R. E.; Schmidbaur, H. *Inorg. Chem.* **1992**, *35*, 1399. (h) Schmidbaur, H.; Kolb, A.; Bissinger, P. *Inorg. Chem.* **1992**, *31*, 4370.
(43) Yang, Y.; Ramamoorthy, V.; Sharp, P. R. *Inorg. Chem.* **1993**, *32*, 1946.
(44) Wang, S.-G.; Schwartz, W. H. E. *J. Am. Chem. Soc.* **2004**, *126*, 1266.
(45) Bardaji, M.; Laguna, A.; Orera, V. M.; Villacampa, M. D. *Inorg. Chem.* **1998**, *37*, 5125.
(46) Chen, J.; Jiang, T.; Wei, G.; Mohamed, A. A.; Homrighausen, C.; Bauer, J. A. K.; Bruce, A. E.; Bruce, M. R. M. *J. Am. Chem. Soc.* **1999**, *121*, 9225.
(47) Bunge, S. D.; Just, O.; Rees, W. S., Jr. *Angew. Chem., Int. Ed.* **2000**, *39*, 3082.
(48) Chiari, R.; Pionesava, O.; Tarantelli, T.; Zanazzi, P. F. *Inorg. Chem.* **1985**, *24*, 366.
(49) (a) Kappen, T. G. M. M.; Schlebos, P. P. J.; Bour, J. J.; Bosman, W. P.; Smits, J. M. M.; Beurskens, P. T.; Steggerda, J. J. *Inorg. Chem.* **1994**, *33*, 754. (b) Kappen, T. G. M. M.; Schlebos, P. P. J.; Bour, J. J.; Bosman, W. P.; Beurskens, G.; Smits, J. M. M.; Beurskens, P. T.; Steggerda, J. J. *Inorg. Chem.* **1995**, *34*, 2121.
(50) Teo, B. K.; Zhang, H.; Shi, X. *Inorg. Chem.* **1994**, *33*, 4086.
(51) Cerrada, E.; Contel, M.; Valencia, A. D.; Laguna, M.; Gelbrich, T.; Hursthouse, M. B. *Angew. Chem., Int. Ed.* **2000**, *39*, 2353.
(52) Schmidbaur, H. *Gold Bull.* **2000**, *33*, 3.
(53) Schmidbaur, H. *Nature* **2001**, *413*, 31.
(54) Pyykkö, P.; Runeberg, N.; Mendizabal, F. *Chem. Eur. J.* **1997**, *3*, 1451.
(55) Pyykkö, P.; Mendizabal, F. *Chem. Eur. J.* **1997**, *3*, 1458.
(56) Pyykkö, P. *Chem. Rev.* **1997**, *97*, 597.

Table 1. Au−Au Bond Distances (pm) and Au−Au−Au Bond Angles (°) for Some Cyclic Square Planar Tetranuclear Au(I) Complexes

cluster	*R*(Au–Au)	∠Au–Au–Au	ref
$[(dppm)_2Au_4(3,5\text{-}Ph_2Pz)_2]^{2+}$	313.2 (325.5)	84.0 (93.5)	32a
$[Au_4(ArNC(H)NC_6H_4\text{-}4\text{-}OMe)_4]$	291.4 (297.5)	70.9 (109.1)	32b
$[Au_4(ArNC(H)NC_6H_3\text{-}3,5\text{-}Cl)_4]$	286.6 (297.0)	88.3 (91.5)	32b
$[Au_4(ArNC(H)NC_6H_4\text{-}4\text{-}Me)_4]$	303.6 (303.3)	63.6 (120.5)	32b
$[Au(\mu\text{-}3,5\text{-}^tBu_2\text{-}pz)]_4$	312.5 (318.2)	76.4 (102.8)	34
	311.7 (316.9)	78.8 (100.6)	
$[(PMe_3Au)_2(\mu\text{-TATG})]_2^{2+}$	310.6 (315.8)	89.7 (90.2)	35
$[Au(\mu\text{-}PMes_2]_4$	334.1 (344.5)		38
$[(o\text{-tol})P\{Au(PPh_3)\}_4]^{2+}$	298.4 (297.8)		42e
$[HC\{Au(PPh_3)\}_4]^+$	293.3 (299.8)		42f
$[P(AuPPh_3)_5]^{2+}$	292.6(295.7)		42g
$[(8\text{-quinolinaminato})\{Au(PPh_3)\}_4]^{2+}$	298.4 (297.8)		42h
$[Au_4(\mu\text{-dpmp})_2Cl_2]^{2+}$	310.3 (310.6)	67.8 (112.3)	44
$[(Ph_3P)_4Au_4(\mu\text{-}SC_6H_4CH_3)_2]^{2+}$	315.2 (317.3)	87.5 (92.5)	46
$[\{Au[(\mu\text{-}N(SiMe_3)_2]\}]_4$	301.0 (303.6)	90.0 (90.0)	47
$[Au_4(\mu\text{-}CH_3CS_2)_4]$	300.7 (302.0)	66.6 (113.9)	48

interactions are clearly shown in the Au_3 triangle of the phosphido-bridged trinuclear gold(I) complex $[Au(\mu\text{-}PIs_2)]_3$ (Is = 2,4,6,-(*i*-Pr)$_3$C$_6$H$_2$)) with Au−Au distances ranging from 306.6 to 309.7 pm.[38] The cyclic square planar Au_4 moiety is more abundant in tetranuclear gold(I) complexes. Very recently, Fackler's group[32] has reported the structure and luminescence of tetranuclear gold(I) pyrazolate $[(dppm)_2Au_4(3,5\text{-}Ph_2Pz)_2]^{2+}$ and formamidinate $[Au_4(ArNC(H)NAr)_4]$ clusters. The Au−Au bond distances, along with the Au−Au−Au bond angles, for some cyclic square planar tetranuclear Au(I) clusters are compiled in Table 1. The only example of a pentanuclear gold(I) cluster with a cyclic planar structure corresponding to an Au_5 pentagon with very short Au−Au edges (average Au−Au bond distance 270.3 pm) studied so far is the $[Au_5(\mu\text{-Mes})_5]\cdot$ 2THF complex.[25] However, the Au_5 and Ag_5 pentagons coexist in superclusters containing group 10 and 11 metals.[49,50] Interestingly, the structure of a 25-metal atom supracluster $[Pt_2(AuPPh_3)_{10}Ag_{13}Cl_7)]$ consists of two identical icosahedral Pt-centered subunits sharing a single common vertex, which is a silver atom.

The central Pt atoms are "sandwiched" between Au_5 and Ag_5 pentagons, forming all-metal metallocene-like units.[49a] The Au−Au and Ag−Ag bond distances in the nearly perfect metallic pentagons are 287.6−288.5 and 284.2−291.8 pm, respectively. The four-metal pentagons adopt the staggered-eclipsed-staggered configuration in the $[(Ph_3)_{10}Au_{12}Ag_{12}PtCl_7)]^+$ and $[(Ph_3)_{10}Au_{12}Ag_{12}NiCl_7)]^+$ biicosahedral superclusters,[50] with Au−Au bond distances in the Au_5 pentagons of 288.8 and 288.4 pm, respectively, and Ag−Ag bond distances in the Ag_5 pentagons of 292.0 and 288.8 pm, respectively. Finally, cyclic planar hexanuclear gold(I) complexes are very rare. The Au_6 hexagon composes the core structure of the $[Au_6Ag\{\mu\text{-}C_6H_2(CHMe_2)_3\}_6]^+$ complex, incorporating at its center a silver(I) atom, thus, looking like an Au_6Ag wheel with a gold rim.[51] The Au_6 skeleton corresponds to a perfect hexagon, with all six Au−Au bond distances equivalent (279.7 pm) and Au−Au−Au bond angles of 60.0°, while the Au−Ag bond distances, being also equivalent, are 280.3 pm and the Au−Ag−Au bond angles are 60.0°.

In this context, we address here a number of important issues related to the molecular and electronic structures, stabilities, bonding features, and spectroscopic properties of prototypical cyclic hydrosilvers(I), Ag_nH_n, and hydrogolds(I), Au_nH_n, (n = 3−6) and some of their substituted derivatives constituting novel classes of inorganic aromatic species. Why these species are expected to be stable molecules and why they exhibit a perfect planar configuration are questions that we will attempt to answer herein by means of electronic structure calculation methods at the DFT level of theory.

Theoretical Methods

In view of the good performance of density functional theory (DFT), we were instigated to perform DFT calculations at the B3LYP level of theory on all of the compounds we studied using the GAUSSIAN03 program suite.[57] The geometries of all species were fully optimized at the Becke 3-parameter hybrid functional[58,59] combined with the Lee−Yang−Parr[60] correlation functional, abbreviated as B3LYP level of density functional theory, using the LANL2DZ basis set. Initial structures obtained at the B3LYP/LANL2DZ level were further optimized at the same level of theory but using a larger basis set consisting of the LANL2DZ basis set for the metal atoms and the cc-pVQZ basis set for the H atoms. Moreover, one additional f-type polarization function ($\alpha_f = 0.75$) is implemented for the Au atoms. It has been found that such polarization functions are required for precisely describing the aurophilic interaction.[54−56] Full geometry optimization was performed for each structure using Schlegel's analytical gradient method,[61] and the attainment of the energy minimum was verified by calculating the vibrational frequencies that result in the absence of imaginary eigenvalues. All the stationary points have been identified for minima (number of imaginary frequencies NIMAG = 0) or transition states (NIMAG = 1). The vibrational modes and the corresponding frequencies are based on a harmonic force field. This was achieved with the SCF convergence on the density matrix of at least 10^{-9} and the rms force less than 10^{-4} au. All bond lengths and bond angles were optimized to better than 0.001 Å and 0.1°, respectively. The computed electronic energies, the enthalpies of reactions, $\Delta_R H_{298}$ and the free energies, ΔG_{298}, were corrected to constant pressure and 298 K for zero point energy (ZPE) differences and for the contributions of the translational, rotational, and vibrational partition functions. The natural bond orbital (NBO) population analysis was performed using Weinhold's methodology.[62,63] Magnetic shielding tensors have been computed with the GIAO (gauge-including atomic orbitals) DFT method,[64,65] as implemented in the GAUSSIAN03 series of programs,[57] employing the B3LYP level of theory. Nucleus-independent chemical shifts (NICS) values were computed at the B3LYP/LANL2DZ level according to the procedure described by Schleyer et al.[66] The magnetic shielding tensor element was calculated for a host atom located at the center of the ring. Time-dependent density

(57) Frisch, M. J.; Trucks, G. W.; Schlegel, H. B.; Scusseria, G. E.; Robb, M. A.; Cheeseman, J. R.; Zakrzewski, V. G.; Montgomery, J. A.; Vreven, T.; Kudin, K. N.; Burant, J. C.; Millan, J. M.; Iyengar, S. S.; Tomasi, J.; Barone, V.; Mennucci, B.; Cossi, M.; Scalmani, G.; Rega, N.; Petersson, G. A.; Nakatsuji, H.; Hada, M.; Ehara, M.; Toyota, K.; Fukuda, R.; Hasegawa, J.; Ishida, M.; Nakajima, T.; Honda, Y.; Kitao, O.; Nakai, H.; Klene, M.; Li, X.; Knox, J. E.; Hratchian, H. P.; Cross, J. B.; Adamo, C.; Jaramillo, J.; Gomperts, R.; Stratmann, R. E.; Yazyev, O.; Austin, A. J.; Cammi, R.; Pomelli, C.; Ochterski, J. W.; Ayala, P. Y.; Morokuma, K.; Voth, G. A.; Salvador, P.; Dannenberg, J. J.; Zakrzewski, V. G.; Dapprich, S.; Daniels, A. D.; Strain, M. C.; Farkas, O.; Malick, D. K.; Rabuck, A. D.; Raghavachari, K.; Foresman, J. B.; Ortiz, J. V.; Cui, Q.; Baboul, A. G.; Clifford, S.; Cioslowski, J.; Stefanov, B. B.; Liu, G.; Liashenko, A.; Piskorz, P.; Komaromi, I.; Martin, R. L.; Fox, D. J.; Keith, T.; Al-Laham, M. A.; Peng, C. Y.; Nanayakkara, A.; Challacombe, M.; Gill, P. M. W.; Johnson, B.; Chen, W.; Wong, M. W.; Gonzalez, C.; Pople, J. A. *Gaussian 03*, revision B.02; Gaussian, Inc.: Pittsburgh, PA, 2003.
(58) Becke, A. D. *J. Chem. Phys.* **1992**, *96*, 215.
(59) Becke, A. D. *J. Chem. Phys.* **1993**, *98*, 5648.
(60) Lee, C.; Yang, W.; Parr, R. G. *Phys. Rev. B* **1998**, *37*, 785.
(61) Schlegel, H. B. *J. Comput. Chem.* **1982**, *3*, 214.
(62) Reed, A. E.; Curtiss, L. A.; Weinhold, F. *Chem. Rev.* **1988**, *88*, 899−926.
(63) Weinhold, F. In *The Encyclopedia of Computational Chemistry*; Schleyer, P. v. R., Ed.; John Wiley & Sons: Chichester, 1998; 1792−1811.
(64) Ditchfield R. *Mol. Phys.* **1974**, *27*, 789.
(65) Gauss, J. *J. Chem. Phys.* **1993**, *99*, 3629.
(66) Schleyer, P. v. R.; Maerker, C.; Dransfeld, A.; Jiao, H.; Hommes, N. J. R. v. R. *J. Am. Chem. Soc.* **1996**, *118*, 6317.

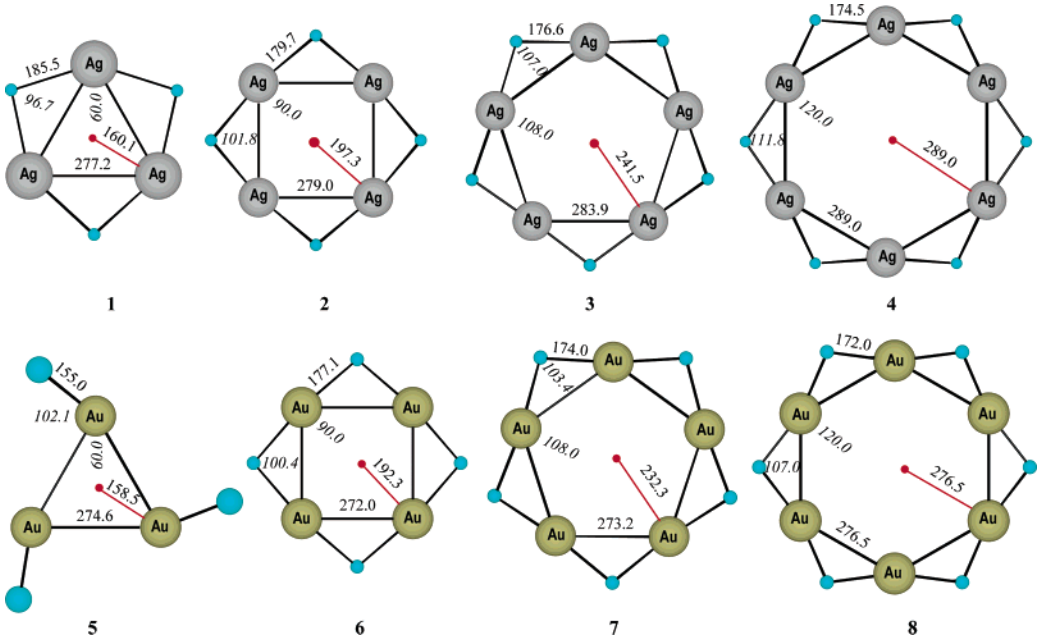

Figure 1. Equilibrium geometries for the cyclic planar M_nH_n (M = Ag, Au; n = 3−6) molecules computed at the B3LYP level of theory using the LANL2DZ basis set for Ag atoms, the LANL2DZ basis set plus one f polarization function (α_f = 0.75) for Au atoms, and the cc-pVQZ basis set for H atoms.

functional theory (TD-DFT)[67] calculations were performed on the equilibrium ground-state geometries employing the same density functionals and basis sets used in geometry optimization. The Davidson algorithm was used, in which the error tolerance in the square of the excitation energies and trial-vector orthonormality criterion were set to 10^{-8} and 10^{-10}, respectively. The success of TD-DFT method in calculating excitation energies of transition metal complexes has been demonstrated in several recent studies.[68] Vertical electron detachment energies from the lowest-energy singlet structures of the cyclic hydrometals were calculated using the outer valence Green function (OVGF) method,[69] incorporated in Gaussian03, and the LANL2DZ basis set.

Results and Discussion

Equilibrium Geometries of the Cyclic Silver(I) and Gold(I) Hydrides. The equilibrium geometries of the cyclic M_nH_n (M = Ag, Au; n = 3−6) molecules computed at the B3LYP level of theory are shown in Figure 1.

It can be seen that all hydrometals, except Au_3H_3, involve bridging hydride ligands which form, with the bridged metal atoms, perfect isosceles triangles. As far as we know, these molecules constitute the first examples of hydrido-bridged polynuclear transition metal compounds that contain perfectly symmetric hydrido-bridges. The computed Ag−H and Au−H bond lengths of the hydrido-bridges found at the regions of 174.5−185.5 pm and 155.0−177.1 pm, respectively, decrease when going from the three- to six-membered all-metal rings. Surprisingly, in the Au_3H_3 molecule, the hydride ligands are terminal exhibiting, as expected, a much shorter Au−H bond length of 155.0 pm. The Ag−H and Au−H bond lengths of the AgH and AuH monomers computed at the same level of theory, predicted to be 162.5 and 152.8 pm, respectively, are in excellent agreement with the experimental values of 161.8 and 152.4 pm.[70] The same also holds true for the computed D_0(Ag−H) and D_0(Au−H) bond dissociation energies of 2.22 and 3.02 eV, respectively; the experimental values are 2.28 and 3.32 eV, respectively.[70] The computed harmonic vibrational ν(Ag−H) and ν(Au−H) frequencies of 1768.6 and 2316.9 cm^{-1}, respectively, are also in excellent agreement with the experimental values of 1760 and 1305 cm^{-1}. The high accuracy and reliability of the computed M−H (M = Ag or Au) bond lengths, dissociation energies, and vibrational frequencies strongly suggests the combination of the B3LYP approach with the selected basis sets to adequately describe the structural, energetic, spectroscopic, and electronic properties of the M_nH_n (M = Ag, Au; n = 3−6) molecules, which are characterized by the closed-shell d^{10}−d^{10} intermetallic interactions.

The computed intermetallic Ag−Ag and Au−Au distances ranging from 272.2 to 289.0 pm and 274.6 to 276.5 pm, respectively, are indicative of strong closed-shell metal−metal interactions. The Ag−Ag and Au−Au distances are less than those expected by the van der Waals radii for Ag (344.0 pm)[71] and Au (322 pm).[71] Considering that substituents, L, on the periphery of M_nL_n (M = Ag, Au; L = a bridging ligand; n = 3−6) molecules affect the extent of metallophilic interactions and, consequently, the M···M separation distances, the computed Ag−Ag and Au−Au bond distances compare well with those

(67) (a) van Gisbergen, S. J. A.; Kootstra, F.; Schipper, P. R. T.; Gritsenko, O. V.; Snijders, J. G.; Baerends, E. J. *Phys. Rev. A* **1998**, *57*, 1556. (b) Jamorski, C.; Casida, M. E.; Salahud, D. R. *J. Chem. Phys.* **1996**, *104*, 5134. (c) Bauernschmitt, R.; Ahlrichs, R. *Chem. Phys. Lett.* **1996**, *256*, 454.

(68) (a) van Gisbergen, S. J. A.; Groeneveld, J. A.; Rosa, A.; Snijders, J. G.; Baerends, E. J. *J. Phys. Chem. A* **1999**, *103*, 6835. (b) Rosa, A.; Baerends, E. J.; van Gisbergen, S. J. A.; van Lenthe, E.; Groeneveld, J. A.; Snijders, J. G. *J. Am. Chem. Soc.* **1999**, *121*, 10356. (c) Boulet, P.; Chermette, H.; Daul, C.; Gilardoni, F.; Rogemond, F.; Weber, J.; Zuber, G. *J. Phys. Chem. A* **2001**, *105*, 885.

(69) (a) Cederbaum, L. S. *J. Phys. B* **1975**, *8*, 290. (b) von Niessen, W.; Shirmer, J.; Cederbaum, L. S. *Comput. Phys. Rep.* **1984**, *1*, 57. (c) Zakrzewski, V. G.; von Niessen, W. *J. Comput. Chem.* **1993**, *14*, 13. (d) Zakrzewski, V. G.; Ortiz, J. V. *Int. J. Quantum. Chem.* **1995**, *53*, 583. (e) Ortiz, J. V.; Zakrzewski, V. G.; Dolgunitcheva, O. In *Conceptual Trends in Quantum Chemistry*; Kryachko, E. S., Ed.; Kluwer: Dordrecht, 1997; Vol. 3, p 463.

(70) Hubert, K. P.; Herzberg, G. *Molecular spectra and Molecular Structure. IV. Constants of Diatomic Molecules*; Van Nostrand Reinhold Company: New York, 1979.

(71) Bondi, A. *J. Phys. Chem.* **1964**, *68*, 441.

found experimentally in a variety of M_nL_n clusters discussed in the Introduction. Compare, for example, the Ag−Ag bond distances of 272.5, 276.9, and 277.2 pm in the Ag_3 triangle found in the homoleptic carbene-bridged $[(\mu\text{-NHC})_3Ag_3]^{3+}$ species,[19] as well as the Ag−Ag bond distances of 285.1 pm found in the four-membered $[Ag_4]^{4+}$ planar parallelogram of the homoleptic carbene-bridged $[(\mu\text{-NHC})_4Ag_4]^{4+}$ species.[22] Analogous comparisons should be made for the rest of the $[M_nH_n]$ (M = Ag, Au; n = 3−6) systems.

Noteworthy is the perfectly planar configuration of high symmetry adopted by all cyclic hydrosilver(I) and hydrogold(I) analogues of the corresponding cyclic hydrocarbons. Also noteworthy is the perfectly planar configuration of high symmetry characterizing many of the analogous M_nL_n (M = Ag, Au; L = a bridging ligand; n = 3−6) molecules experimentally studied so far.[14−51] In this context, the $[M_nH_n]$ (M = Ag, Au; n = 3−6) molecules could be considered as the prototypical molecules for a whole series of cyclic all-metal-containing metallacycles, thus establishing an important new field in chemistry.

Searching the potential-energy surfaces of the $[M_nH_n]$ (M = Ag, Au; n = 3−6) systems, novel low-energy 3D structures were also identified as local minima. The equilibrium geometries of the 3D hydrosilver(I) and hydrogold(I) compounds computed at the B3LYP level of theory are shown in Figure 2. The total electronic energies and the relative energies of the 2D and 3D structures of the hydrosilvers(I) and hydrogolds(I) are summarized in Table 2.

It can be seen that both hydrosilver(I) and hydrogold(I) clusters adopt similar 3D structures with the M_n (n = 4, 5, and 6) cores exhibiting trigonal pyramidal (n = 4), square pyramidal (n = 5), and octahedral (n = 6) stereochemistry. In the trigonal pyramidal structures, one of the hydride ligands is triply bonded to metal(I) atoms located over the center of the basal trigonal plane of the pyramid. The rest of the hydride ligands form three bridges in the Ag_4H_4 but are terminal in the Au_4H_4 molecules. The basal plane of the trigonal pyramid corresponds to an equilateral triangle with Ag−Ag and Au−Au edges of 290.7 and 298.8 pm, respectively. The apical Ag or Au atoms are also strongly bonded to the basal metal atoms forming shorter Ag−Ag and Au−Au bonds with bond lengths of 283.9 and 279.8 pm, respectively. These structures closely resemble those resulting from the interaction of the equilateral Ag_3 or Au_3 triangles with Ag(I) or Au(I), respectively, as it was observed experimentally forming sandwichlike complexes analogous to metallocenes.[28] The same also holds true for the square pyramidal and octahedral M_nH_n 3D clusters. In the square pyramidal structures, the electron-rich Ag_4 (average Ag−Ag bond distances = 283.7 pm) and Au_4 (average Au−Au bond distances = 272.8 pm) square basal planes interact with the AgH and AuH (average Au−Au bond distances = 315.8 pm) Lewis acids, respectively, along the C_4 axis, thus occupying the apical position of the pyramid. The Ag−Ag and Au−Au separation distances between the apical and the basal metal atoms range from 300.6 to 312.1 pm and 295.7 to 337.0 pm, respectively. In the octahedral structures, the equatorial electron-rich Ag_4 and Au_4 perfect squares with Ag−Ag and Au−Au edges of 291.1 and 273.6 pm, respectively, interact from both sites with two molecules of the AgH and AuH Lewis acids along the C_4 axis, thus affording the octahedral coordination. Interestingly, the Ag_6 core adopts a perfect octahedral structure with four hydrido-bridged ligands triply bridging the Ag(I) atoms of the trigonal faces of the octahedron in trans positions. On the other hand, the Au_6 core adopts a tetragonally distorted (elongated) octahedron with the Au−Au separation distances between the axial and the equatorial Au(I) atoms ranging from 291.1 to 339.9 pm. Looking at the 3D structure of Au_6H_6 cluster, one can easily see the perfect square planar $Au_4(\mu\text{-H})_4$ moiety loosely associated with two AuH molecules along its C_4 axis. It should be stressed that all 3D structures of hydrosilvers(I) and hydrogolds(I) were found to be less stable than the 2D planar ones by 43.1−53.8 and 34.1−59.0 kcal/mol, respectively. Why the 2D planar structures are stabilized with respect to the 3D ones is a question that we will attempt to answer in the following on the grounds of the electronic structure and bonding properties of the *cyclo*-M_nH_n (M = Ag or Au; n = 3−6) molecules computed by DFT.

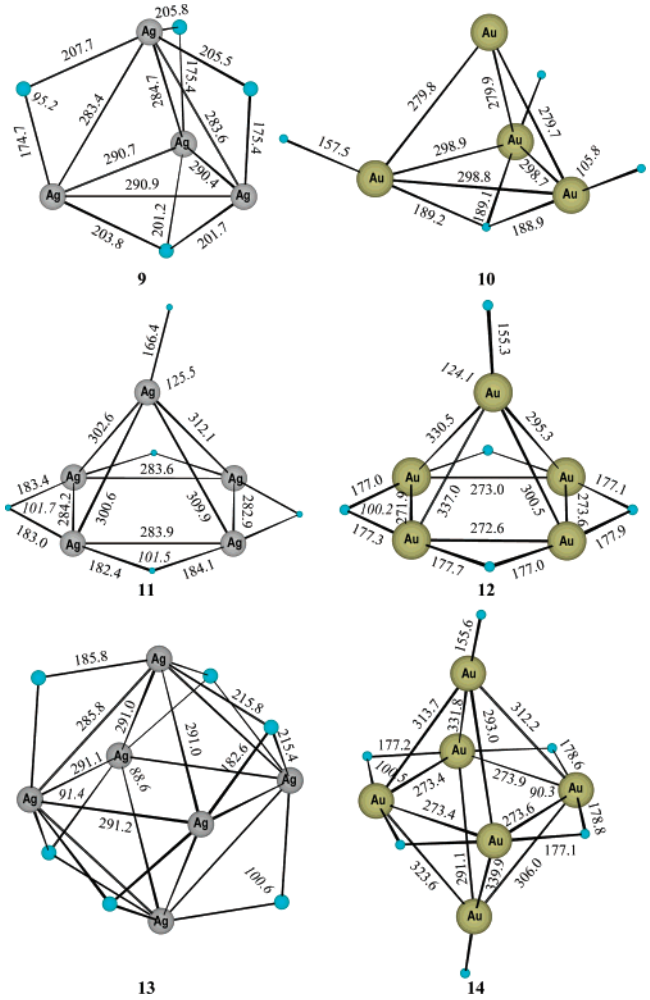

Figure 2. Equilibrium geometries for the 3D structures of the M_nH_n (M = Ag, Au; n = 3−6) molecules computed at the B3LYP level of theory using the LANL2DZ basis set for Ag atoms, the LANL2DZ basis set plus an f polarization function (α_f = 0.75) for Au atoms, and the cc-pVQZ basis set for H atoms.

Stability of the Cyclic Hydrosilvers(I) and Hydrogolds(I). Let us first examine the stability of the cyclic planar hydrometals M_nH_n (M = Ag or Au; n = 3−6) with respect to (i) their dissociation to the MH monomers, (ii) their dissociation to free M and H atoms in their ground states, and (iii) their

Table 2. Total Electronic Energies (Hartrees) and Relative Energies (kcal/mol) of the 2D and 3D Structures of the $[M_nH_n]$ (M = Ag, Au; n = 3−6) Hydrosilver(I) and Hydrogold(I) Molecules Computed at the B3LYP Level.

compound (2D)	E^a	compound (3D)	E^a	ΔE
$Ag_3H_3(D_{3h})$	−439.125981 (−439.110494)[b]			
$Ag_4H_4(D_{4h})$	−585.551501 (−585.524557)	Ag_4H_4	−585.482807 (−585.463338)	43.1 (38.4)
$Ag_5H_5(D_{5h})$	−731.959049 (−731.922042)	Ag_5H_5	−731.876436 (−731.873036)	51.8 (30.8)
$Ag_6H_6(D_{6h})$	−878.357067 (−878.311215)	Ag_6H_6	−878.271327 (−878.242415)	53.8 (43.2)
$Au_3H_3(D_{3h})$	−408.219089 (−408.183160)			
$Au_4H_4(D_{4h})$	−544.337024 (−544.288361)	Au_4H_4	−544.273428 (−544.229071)	39.9 (37.2)
$Au_5H_5(D_{5h})$	−680.461782 (−680.396140)	Au_5H_5	−680.407493 (−680.350107)	34.1 (28.9)
$Au_6H_6(D_{6h})$	−816.573194 (−816.491195)	Au_6H_6	−816.479142 (−816.412669)	59.0 (49.3)

[a] Total electronic and relative energies computed at the B3LYP level using the LANL2DZ basis set for Ag atoms, the LANL2DZ basis set plus an f polarization function ($\alpha_f = 0.75$) for Au atoms, and the cc-pVQZ basis set for H atoms. [b] Figures in parentheses are the total electronic and relative energies computed at the B3LYP/LANL2DZ level of theory.

Table 3. Binding Energies ΔE_1, ΔE_2, and ΔE_3 (kcal/mol) of the Cyclic *cyclo*-M_nH_n (M = Ag or Au; n = 3−6) Hydrometals, Computed at the B3LYP Level of Theory Using the LANL2DZ Basis Set for Ag Atoms, the LANL2DZ Basis Set Plus an f Polarization Function ($\alpha_f = 0.75$) for Au Atoms, and the cc-pVQZ Basis Set for H Atoms

cluster	ΔE_1[a]	ΔE_1/mol MH	ΔE_2[b]	ΔE_3[c]
$Ag_3H_3(D_{3h})$	−61.3 (−59.9)[d]	20.4 (20.0)	−215.2 (−214.7)	−59.1 (−55.2)
$Ag_4H_4(D_{4h})$	−113.2 (−107.5)	28.3 (26.9)	−318.4 (−310.1)	−110.3 (−101.2)
$Ag_5H_5(D_{5h})$	−153.9 (−144.6)	30.8 (28.9)	−410.3 (−397.8)	−150.3 (−137.0)
$Ag_6H_6(D_{6h})$	−188.5 (−176.6)	31.4 (29.4)	−496.3 (−480.4)	−183.9 (−167.6)
$Au_3H_3(D_{3h})$	−37.5 (−35.2)	12.5 (11.7)	−246.4 (−230.3)	−90.3 (−73.9)
$Au_4H_4(D_{4h})$	−78.1 (−74.6)	19.5 (18.7)	−356.7 (−334.8)	−148.7 (−126.1)
$Au_5H_5(D_{5h})$	−123.1 (−115.7)	24.6 (23.1)	−471.3 (−440.9)	−211.3 (−180.0)
$Au_6H_6(D_{6h})$	−159.7 (−148.8)	26.6 (24.8)	−577.6 (−539.0)	−265.3 (−226.2)

[a] $\Delta E_1 = E(M_nH_n) - nE(MH)$. [b] $\Delta E_2 = E(M_nH_n) - [nE(M) + nE(H)]$. [c] $\Delta E_3 = E(M_nH_n) - [nE(M) + (n/2)E(H_2)]$. [d] Figures in parentheses are the binding energies computed at the B3LYP/LANL2DZ level.

dissociation to the standard states of their elements, e.g. M and H_2. The calculated binding energies are compiled in Table 3.

It can be seen that all cyclic planar hydrosilvers(I) and hydrogolds(I) are predicted to be bound with respect to their dissociation either to the MH monomers or to free M and H atoms in their ground states. Notice that the formation of the cyclic hydrosilvers(I) from the association of the monomeric AgH species corresponds to a more exothermic process than the formation of the cyclic hydrogolds(I) from the AuH monomers. However, the opposite is true for the formation energy of the cyclic M_nH_n (M = Ag or Au; n = 3−6) molecules from their constituent atoms. This could be attributed to the lower D_0(Ag−H) bond-dissociation energy (51.2 kcal/mol) than D_0(Au−H) (69.6 kcal/mol) computed at the B3LYP level of theory. Noteworthy are the computed ΔE_1 per mole of monomers, MH, ranging from 19.5 to 31.4 kcal/mol, which account for the sum of the M−M and M−H-M bond energies. Considering that in the *cyclo*-Au_3H_3 molecule no hydrogen bonds are formed, the computed ΔE_1 per mole of AuH of 12.5 kcal/mol corresponds to the strength of the Au−Au interactions, a value characteristic for the strength of the aurophilic interactions.

Importantly, the formation of the *cyclo*-M_nH_n species from their elements M(s) and H_2(g) corresponds to an exothermic process (Table 3), indicating that these species could be formed in MS of gold vapor sputtered with hydrogen or by the normal spectroscopic approach of deposition of the metal in a hydrogen matrix. The computed exothermicities, ranging from −59.1 to −265.3 kcal/mol, are higher for the hydrogold(I) than for the hydrosilver(I) species. It is worth noting that the formation of the monomeric AuH(g) species by reacting Au(g) and H_2(g) is also an exothermic process, the computed exothermicity being −17.6 kcal/mol, thus accounting for the generation of AuH(g) species in the gas phase. In contrast, the respective gas-phase reaction generating the AgH(g) species was predicted to be an almost thermoneutral process.

To understand deeper the planarity and structural integrity of the *cyclo*-M_nH_n (M = Ag or Au; n = 3−6) hydrometals the most relevant valence molecular orbitals and the electronic and bonding properties have been analyzed.

Electronic and Bonding Properties of the Cyclic Hydrosilvers(I) and Hydrogolds(I). The valence-shell electron configurations of the *cyclo*-M_nH_n (M = Ag or Au; n = 3−6) molecules are listed in Table 4.

The *cyclo*-$Ag_3(\mu\text{-H})_3$ and *cyclo*-Au_3H_3 molecules with 36 valence electrons have singlet $^1A_1'$ and ^1A electronic states for their ground D_{3h} and C_{3h} structures, respectively. The *cyclo*-$Ag_4(\mu\text{-H})_4$ and *cyclo*-$Au_4(\mu\text{-H})_4$ molecules with 48 valence electrons have a singlet $^1A_{1g}$ electronic state for their ground D_{4h} structures. The *cyclo*-$Ag_5(\mu\text{-H})_5$ and *cyclo*-$Au_5(\mu\text{-H})_5$ molecules with 60 valence electrons also have a singlet $^1A_1'$ electronic state for their ground D_{5h} structures. Finally, the *cyclo*-$Ag_6(\mu\text{-H})_6$ and *cyclo*-$Au_6(\mu\text{-H})_6$ molecules with 84 valence electrons have a singlet $^1A_{1g}$ electronic state for their ground D_{6h} structures. Surprisingly, despite each of the all-metal rings (except the three-membered ones) adopting the same electronic state and symmetry for both the silver and gold metals, the sequence of the occupied molecular orbitals (MOs) is different. However, for each metallic ring, the frontier molecular orbitals (FMOs) correspond to MOs of the same symmetry.

Generally, all cyclic hydrosilvers(I) and hydrogolds(I) studied exhibit similar bonding properties. The most relevant valence molecular orbitals of selected *cyclo*-Ag_nH_n and *cyclo*-Au_nH_n (n = 3−6) hydrometals are shown in Figures 3 and 4.

Perusal of Figures 3 and 4 reveals that all metallacycle rings exhibit a composite bonding mode involving σ, π, and δ

Table 4. Valence Shell Electron Configurations for the $[M_nH_n]$ (M = Ag, Au; $n = 3-6$) Hydrosilver(I) and Hydrogold(I) Molecules Computed at the B3LYP Level

M_nH_n	symmetry	valence electrons	state	electron configuration
Ag_3H_3	D_{3h}	36	$^1A_1'$	····· $(2a_2'')^2(2e'')^4(5e')^4(1a_1'')^2(6e')^4(3e'')^4(2a_2')^2(5a_1')^2(7e')^4$
Ag_4H_4	D_{4h}	48	$^1A_{1g}$	·····$(3e_g)^4(3b_{1g})^2\ (3b_{1g})^2(6e_u)^4(2b_{2u})^2(1a_{1u})^2(4b_{1g})^2(2a_{2g})^2(5a_{1g})^2(3b_{2g})^2(7e_u)^4$
Ag_5H_5	D_{5h}	60	$^1A_1'$	····· $(3e_1'')^4(3e_2'')^4(6e_2')^4(6e_1')^4(1a_1'')^2(2a_2')^2(5a_1')^2(7e_2')^4(7e_1')^4$
Ag_6H_6	D_{6h}	84	$^1A_{1g}$	····· $(3e_{1g})^4(2b_{2g})^2(3b_{1u})^2(6e_{1u})^4(1a_{1u})^2(4b_{1u})^2(2a_{2g})^2(3b_{2u})^2(5a_{1g})^2(7e_{1u})^4(7e_{2g})^4$
Au_3H_3	C_{3h}	36	$^1A'$	····· $(2a'')^2(2e'')^4(5e')^4(6a')^2(3a'')^2(6e')^4(3e'')^4(7a')^2(7e')^4$
Au_4H_4	D_{4h}	48	$^1A_{1g}$	···· $(2e_g)^4(5a_{1g})^2(3b_{1g})^2(6e_u)^4(3e_g)^4(3b_{2g})^2(1a_{1u})^2(1b_{2u})^2(4b_{1g})^2(2a_{2g})^2(7e_u)^4$
Au_5H_5	D_{5h}	60	$^1A_1'$	····· $(6e_1')^4(3e_1'')^4(5a_1')^2(6e_2')^4(3e_2'')^4(1a_1'')^2(2a_2')^2(7e_1')^4(7e_2')^4$
Au_6H_6	D_{6h}	84	$^1A_{1g}$	····· $(3e_{1g})^4(6e_{2g})^4(3e_{2u})^4(5a_{1g})^2(3b_{1u})^2(2b_{2g})^2(1a_{1u})^2(4b_{1u})^2(2a_{2g})^2(7e_{1u})^4(7e_{2g})^4$

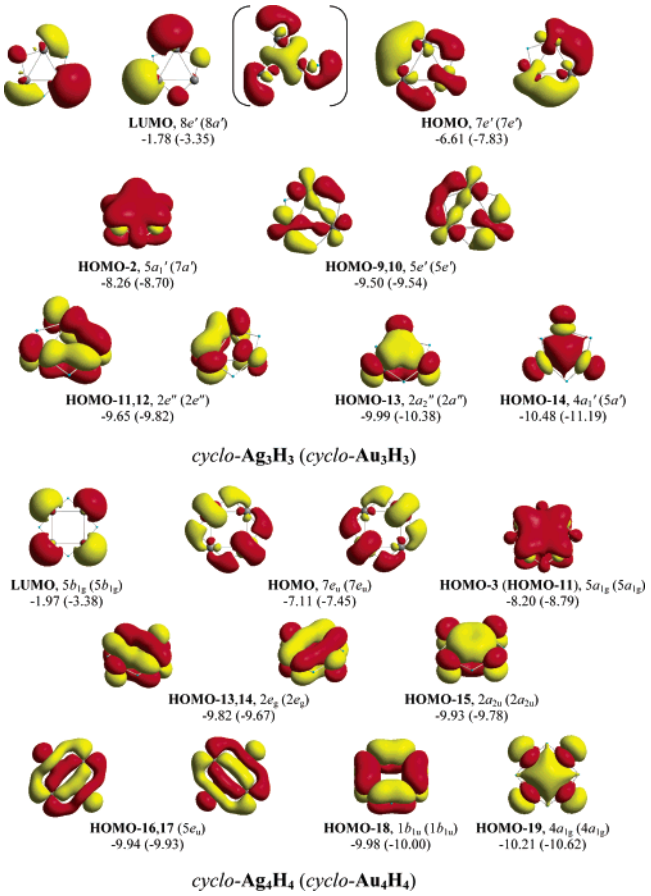

Figure 3. The most-relevant valence molecular orbitals of the *cyclo*-Ag_3H_3 (*cyclo*-Au_3H_3) and *cyclo*-Ag_4H_4 (*cyclo*-Au_4H_4) hydrometals.

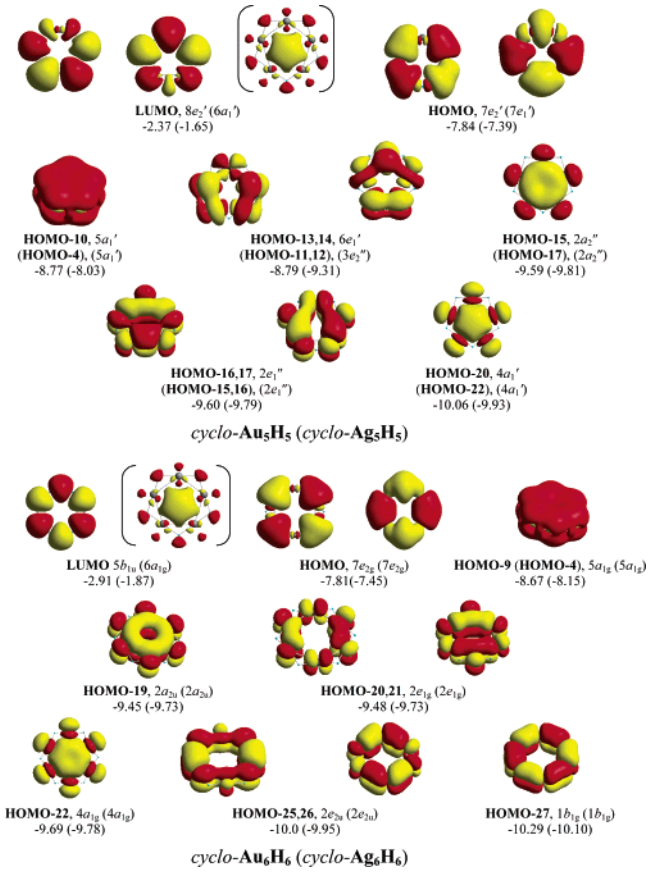

Figure 4. The most-relevant valence molecular orbitals of the *cyclo*-Au_5H_5 (*cyclo*-Ag_5H_5) and *cyclo*-Au_6H_6 (*cyclo*-Ag_6H_6) hydrometals.

components. Noteworthy is the presence of highly delocalized π- and δ-type MOs, such as the HOMO-2 (δ-MO), HOMO-11, HOMO-12, and HOMO-13 (π-MOs) for the three-membered rings (Figure 3), resulting from the bonding interaction of the *n*d AOs of the ring Ag(I) or Au(I) atoms similar to the π-type MOs ($p\pi-p\pi$ overlap) of the corresponding aromatic hydrocarbons, which support a ring current. Moreover, there are also highly delocalized σ-type MOs, such as the HOMO-14, HOMO-19, HOMO-20, and HOMO-22 for the three-, four-, five-, and six-membered rings, respectively (Figures 3 and 4), resulting from the bonding interaction of the *n*d AOs ($nd\sigma-nd\sigma$ overlap) of the ring Ag(I) or Au(I) atoms. The delocalized σ and π electron density in the rings could probably account for the observed equivalence of the Ag−Ag and Au−Au bonds in the all Ag(I) and Au(I) rings of hydrosilvers(I) and hydrogolds(I). Moreover, the extra stabilization of the planar 2D structures with respect to the 3D ones could be associated with the cyclic delocalization of electron density, which is a characteristic feature of aromaticity.

Selected electronic parameters of the cyclic hydrometals M_nH_n (M = Ag or Au; $n = 3-6$) have been collected in Table 5.

The high stability of the *cyclo*-Ag_nH_n and *cyclo*-Au_nH_n rings is also reflected on the high $\epsilon_{LUMO}-\epsilon_{HOMO}$ energy gap, the so-called global hardness, η. According to the computed η values, the stability of the metallic rings increases from the three- to four- and five-membered rings and then slightly decreases in the six-membered rings. The high stability of the three-, four-, five-, and six-membered Ag_n(I) and Au_n(I) rings is reflected on several structurally characterized complexes involving the respective rings.[14−51] The relative hardness, $\Delta\eta$, obtained using the recently introduced isomerization method[72] for a series of C_4H_4X compounds (antiaromatic, nonaromatic, and aromatic)

(72) Schleyer, P. v. R.; Pühlhofer. F. *Org. Lett.* **2002**, *4*, 2873.

Table 5. Selected Electronic Parameters of the Cyclic Hydrometals M_nH_n (M = Ag or Au; $n = 3-6$), Computed at the B3LYP Level of Theory Using the LANL2DZ Basis Set for Ag Atoms, the LANL2DZ Basis Set Plus an f Polarization Function ($\alpha_f = 0.75$) for Au Atoms, and the cc-pVQZ Basis Set for H Atoms

compound	ϵ_{HOMO}	ϵ_{LUMO}	η	$\Delta\eta$	ω^a	*bop*(M–M)	$(n-1)$d/*n*s/*n*p	q_M
$Ag_3H_3(D_{3h})$	−6.61	−1.78	4.83		1.82	0.056	9.94/0.48/0.01	0.57 (0.29)[b]
$Ag_4H_4(D_{4h})$	−7.11	−1.97	5.14 [4.33][c]	0.81	2.00	0.063	9.91/0.55/0.01	0.53 (0.28)
$Ag_5H_5(D_{5h})$	−7.39	−1.65	5.74 [3.69]	2.05	1.78	0.060	9.90/0.58/0.00	0.51 (0.28)
$Ag_6H_6(D_{6h})$	−7.45	−1.87	5.58 [4.05]	1.53	1.95	0.059	9.90/0.59/0.00	0.51 (0.28)
$Au_3H_3(D_{3h})$	−7.83	−3.35	4.48		3.49	0.138	9.75/1.10/0.02	0.13 (0.22)
$Au_4H_4(D_{4h})$	−7.45	−3.38	4.07 [2.32]	1.75	3.60	0.050	9.85/0.74/0.01	0.39 (0.41)
$Au_5H_5(D_{5h})$	−8.10	−2.37	5.73 [3.22]	2.51	2.39	0.042	9.84/0.80/0.00	0.36 (0.41)
$Au_6H_6(D_{6h})$	−7.80	−2.90	4.90 [2.85]	2.05	2.92	0.047	9.83/0.81/0.00	0.35 (0.42)

[a] Electrophilicity index, $\omega = \mu^2/2\eta$, where μ and η are the chemical potential and hardness, respectively, given approximately by the expressions $\mu = (\epsilon_{LUMO} + \epsilon_{HOMO})/2$ and $\eta = (\epsilon_{LUMO} - \epsilon_{HOMO})$. [b] Figures in parentheses are the Mulliken net atomic charges. [c] Figures in brackets refer to the 3D structures.

was found to be a good criterion for aromaticity.[73] Applying this criterion to the planar *cyclo*-Ag_nH_n and *cyclo*-Au_nH_n molecules, it can be suggested that these all-metal rings exhibit aromaticity. The $\Delta\eta$ values computed as the difference between the η values of the 2D and 3D structures $\Delta\eta = \eta(2D) - \eta(3D)$ (Table 5) indicate that the aromaticity follows the trend: *cyclo*-M_5H_5 > *cyclo*-M_6H_6 > *cyclo*-M_4H_4. Moreover, the cyclic hydrogolds(I) exhibit higher aromaticity than their hydrosilver-(I) analogues. It is important to note that the computed $\Delta\eta$ values of the *cyclo*-M_nH_n are comparable to those of aromatic C_4H_4X compounds.[73] The extent of aromaticity of the Cu_nH_n ($n = 3-6$) molecules is also mirrored on the computed[74] electrophilicity index $\omega = \mu^2/2\eta$, where μ and η are the chemical potential and hardness, respectively, given approximately by the expressions $\mu = (\epsilon_{LUMO} + \epsilon_{HOMO})/2$ and $\eta = (\epsilon_{LUMO} - \epsilon_{HOMO})$. The η values also indicate that the *cyclo*-Ag_nH_n and *cyclo*-Au_nH_n molecules are relatively hard nucleophiles which can readily interact with electrophiles, such as H^+, Ag^+, and Tl^+ cations, as was observed experimentally.[28] Notice that the *cyclo*-Au_nH_n molecules, having much higher values of the electrophilicity index, $\omega = \mu^2/2\eta$, than the *cyclo*-Ag_nH_n ones, are stronger nucleophiles, particularly those containing the three- and four-membered rings. It is evident then why the Ag^+ and Tl^+ cations are easily stacked on the Au_3 triangle containing molecules.[28] The same also holds true for the interaction of the Au_4 squares with AuH molecules to yield the 3D structures of the Au_5H_5 and Au_6H_6 clusters.

According to the natural bond orbital (NBO) and Mulliken population analysis (Table 5), there is a significant charge transfer of about 0.43−0.549 and 0.61−0.65 charge units of natural charge from the bridging hydride ligands to Ag(I) and Au(I) metal atoms, respectively. The charge transfer from the terminal hydride ligands to Au(I) in the*cyclo*-Au_3H_3 molecule is much higher (0.87 charge units). The transferred electronic density is accumulated on the vacant *n*s orbitals of the Ag(I) and Au(I) having the $(n-1)d^{10}$ electron configuration. Moreover, the natural electron configurations (Table 5) indicate that there is also promotion of a relatively small amount of electron density from the $(n-1)d^{10}$ to *n*s orbitals amounted to 0.06−0.10 and 0.15−0.25 charge units for the *cyclo*-Ag_nH_n and *cyclo*-Au_nH_n, respectively. This promotion of electron density contributes to the weak intermetallic interactions in the metallic rings. The weak intermetallic interactions are also mirrored on the computed Mulliken bond overlap population *bop*(M−M) (Table 5), ranging from 0.056 to 0.063 and 0.042 to 0.138 for the *cyclo*-Ag_nH_n and *cyclo*-Au_nH_n, respectively. Generally, the Au−Au intermetallic interactions are stronger than the Ag−Ag ones.

Table 6. ^1H, ^{109}Ag, and ^{197}Au Shielding Tensor Elements (σ, ppm) for the *cyclo*-M_nH_n (M = Ag or Au; $n = 3-6$) Hydrometals, Computed at the GIAO/B3LYP Level of Theory Using the LANL2DZ Basis Set for Ag Atoms, the LANL2DZ Basis Set Plus an f Polarization Function ($\alpha_f = 0.75$) for Au Atoms, and the cc-pVQZ Basis Set for H Atoms

	^{109}Ag or ^{197}Au		^1H			
cluster	σ^{iso}	σ^{aniso}	σ^{iso}	σ^{aniso}	(δ, ppm)[a]	NICS(0)
$Ag_3H_3(D_{3h})$	258.6	50.1	27.4	14.3	4.2	−8.9
$Ag_4H_4(D_{4h})$	260.2	74.3	29.9	12.4	1.7	−4.9
$Ag_5H_5(D_{5h})$	263.6	85.7	30.6	18.3	1.0	−0.9
$Ag_6H_6(D_{6h})$	267.5	88.1	31.0	23.3	0.6	−0.3
$Au_3H_3(D_{3h})$	216.6	80.4	31.6	33.8	0.0	−17.8
$Au_4H_4(D_{4h})$	241.5	42.8	31.3	14.9	0.3	−9.0
$Au_5H_5(D_{5h})$	240.9	62.6	32.3	18.8	-0.7	−2.1
$Au_6H_6(D_{6h})$	249.5	58.4	32.4	25.0	-0.8	−0.6

[a] The ^1H chemical shifts (δ, ppm) are equal to the difference between the ^1H shielding of the TMS external reference standard ($\sigma^{iso} = 31.6$ ppm, $\sigma^{aniso} = 9.2$ ppm) and the ^1H shielding of the molecule.

NMR Spectra and Aromaticity of the Cyclic Hydrosilvers-(I) and Hydrogolds(I). Planarity, high stability, bond length equalization, and hardness are conventionally good indicators of aromaticity, but this is restrictive in many examples. To verify further the aromaticity of the *cyclo*-Ag_nH_n and *cyclo*-Au_nH_n molecules, the ^{109}Ag, ^{197}Au, and ^1H NMR shielding tensor elements (σ_{iso} and σ_{aniso}, ppm) were calculated at the GIAO/B3LYP level of theory. The absolute isotropic and anisotropic shielding tensor elements along with the ^1H NMR chemical shifts (δ, ppm) computed from the difference between the shielding of the reference TMS standard and the shielding of the molecule of interest, $\delta = \sigma_{ref} - \sigma$. The results are compiled in Table 6. Notice that the computed NMR spectra of *cyclo*-M_nH_n compounds are predictions, as there are no experimental data available so far, and therefore, they could assist experimentalists in identifying the respective compounds. Moreover, to quantify further the aromaticity/antiaromaticity of the cyclic hydrosilvers(I) and hydrogolds(I), we also applied the magnetic criterion, viz. nucleus-independent chemical shift (NICS), proposed by Schleyer et al.[75] Negative (diatropic) NICS values indicate aromaticity, while positive (paratropic) values imply antiaromaticity. NICS(0) values, which are the negative of the absolute magnetic shielding tensors calculated at the ring centers, are also given in Table 6.

(73) De Proft, F.; Geerlings, P. *Phys. Chem. Chem. Phys.* **2004**, *6*, 242.
(74) Parr, R. G.; v. Szentpály, L.; Liu, S. *J. Am. Chem. Soc.* **1999**, *121*, 1922.
(75) Schleyer, P. v. R.; Maerker, C.; Dransfeld, A.; Jao, H.; Homes, N. v. E. *J. Am. Chem. Soc.* **1996**, *118*, 6317.

Scheme 1

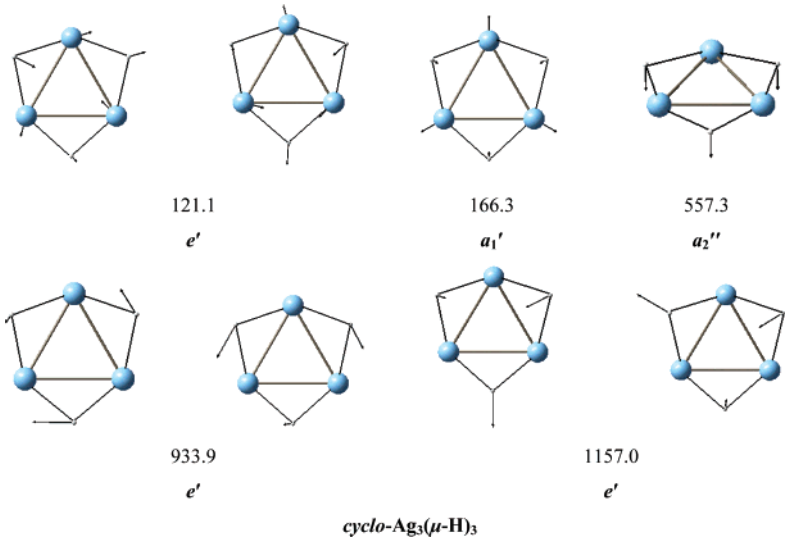

cyclo-$Ag_3(\mu\text{-}H)_3$

It can be seen that all cyclic hydrosilvers and hydrogolds exhibit negative NICS values, the absolute values decreasing along the series of the three- to six-membered all-metal rings. The lowering of the NICS values follows the reverse trend of the ring radius (Figure 1). It seems that the NICS(0) depends on the ring size, and therefore, the low NICS(0) values of the five- and six-membered rings cannot exclude strong aromaticity for these systems as well. Generally, the hydrogolds(I) are more aromatic than the hydrosilvers(I). Noteworthy is the high NICS-(0) value of the *cyclo*-Au_3H_3 molecule (−17.8 ppm) and those of the *cyclo*-Ag_3H_3 (−8.9 ppm) and *cyclo*-Au_4H_4 (−9.0 ppm) molecules, which are comparable to the NICS(0) value of benzene (−9.7 ppm). These findings nicely explain why the Au_3 and Ag_3 triangles, as well as the Au_4 squares, are the more common cores in the structures of polynuclear gold(I) and silver-(I) clusters studied so far.

Vibrational Spectra of the Cyclic Hydrosilvers(I) and Hydrogolds(I). The most characteristic infrared-active vibrational modes of the *cyclo*-M_nH_n (M = Ag or Au; n = 3−6) hydrometals, along with the normal coordinate vectors (arrows), are shown in Schemes 1−4. The harmonic vibrational frequencies and the IR intensities computed at the B3LYP level of theory are listed in detail in the Supporting Information (Table S1).

For *cyclo*-$Ag_3(\mu\text{-}H)_3$ (Scheme 1), the more-intense vibrational modes of e_1' symmetry, absorbing at about 934 and 1157 cm^{-1}, are attributed to the asymmetric vibrations of the bridging hydride ligands around and toward the Ag_3 triangle, respectively. The next-intense vibrational mode of a_2'', absorbing around 557 cm^{-1}, is attributed to the symmetric out-of-plane vibration of the bridging hydride ligands. The vibrations related with the symmetric (a_1') and asymmetric (e') breathing modes of the Ag_3 triangle absorb at about 166 and 121 cm^{-1}, respectively, with the former being IR silent but Raman active.

For *cyclo*-Au_3H_3 (Scheme 2), the more-intense vibrational mode of e_1' symmetry, absorbing at about 2283 cm^{-1}, is attributed to the stretching ν(Au-H) vibrations of the terminal hydride ligands. The next-intense vibrational modes of a′ symmetry, absorbing at 412 and 421 cm^{-1}, are attributed to the bending modes of the terminal hydride ligands. The vibrations related with the symmetric (a_1') and asymmetric (e') breathing

Scheme 2

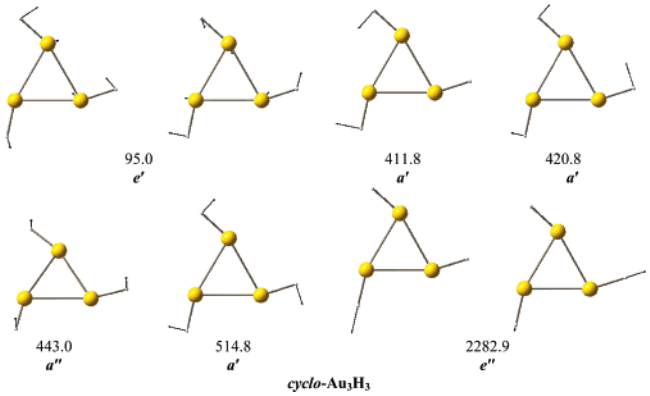

cyclo-Au_3H_3

Scheme 3

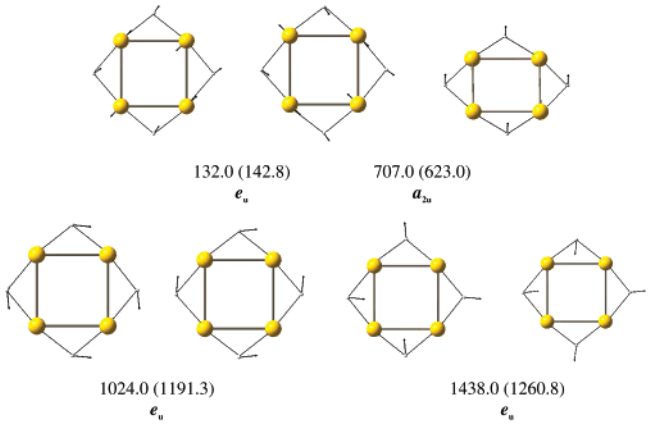

cyclo-$Au_4(\mu\text{-}H)_4$ (*cyclo*-$Ag_4(\mu\text{-}H)_4$)

modes of the Au_3 triangle absorb at about 131 and 95 cm^{-1}, respectively, with the former being only Raman active.

For *cyclo*-$Ag_4(\mu\text{-}H)_4$ and *cyclo*-$Au_4(\mu\text{-}H)_4$ (Scheme 3), the more-intense vibrational modes of e_u symmetry, absorbing at about 1261 and 1438 cm^{-1}, respectively, are attributed to the asymmetric vibrations of the bridging hydride ligands toward the M_4 square. The next-intense vibrational mode of e_u symmetry, absorbing at 1191 and 1024 cm^{-1}, respectively, is that corresponding to the symmetric vibrations of the bridging hydride ligands toward the M_4 square. The a_{2u} vibration at 623

Table 7. Principal Electronic Transitions, Wavelengths (λ) and Oscillator Strengths (f) for the *cyclo*-Ag_nH_n and *cyclo*-Au_nH_n ($n = 3-6$) Molecules Computed at the B3LYP Level of Theory, Using the LANL2DZ Basis Set for Ag Atoms, the LANL2DZ Basis Set Plus an f Polarization Function ($\alpha_f = 0.75$) for Au Atoms, and the cc-pVQZ Basis Set for H Atoms

compound	λ(nm)	f[a]	assignment	compound	λ(nm)	f	assignment
$Ag_3H_3(^1A_1')$	291	0.1062	$7e' \rightarrow 8e'$	$Au_3H_3(^1A')$	324	0.0791	$7e' \rightarrow 8a'$
	237	0.3012	$7e' \rightarrow 6\alpha_1'$		268	0.0101	$6a' \rightarrow 8a'$
	221	0.0574	$5\alpha_1' \rightarrow 8e'$		254	0.0085	$5e' \rightarrow 8a'$
	210	0.0192	$2\alpha_2' \rightarrow 8e'$		237	0.2343	$7e' \rightarrow 8e'$
	204	0.0012	$3e'' \rightarrow 8e'$				
	197	0.0104	$7e' \rightarrow 8e'$				
$Ag_4H_4(^1A_{1g})$	273	0.1130	$7e_u \rightarrow 5b_{1g}$	$Au_4H_4(^1A_{1g})$	356	0.10471	$7e_u \rightarrow 5b_{1g}$
	236	0.4283	$7e_u \rightarrow 6a_{1g}$		304	0.0098	$2b_{2u} \rightarrow 5b_{1g}$
	201	0.0386	$5a_{1g} \rightarrow 3a_{2u}$		287	0.0065	$6e_u \rightarrow 5b_{1g}$
			$2b_{2u} \rightarrow 3a_{2u}$				
$Ag_5H_5(^1A_1')$	246	0.1057	$7e_1' \rightarrow 6\alpha_1'$	$Au_5H_5(^1A_1')$	264	0.1271	$7e_2' \rightarrow 8e_2'$
	228	0.3362	$7e_1' \rightarrow 8e_2'$		253	0.0199	$7e_1' \rightarrow 8e_2'$
	218	0.3319	$7e_2' \rightarrow 8e_2'$		243	0.0104	$3e_2'' \rightarrow 8e_2'$
	239	0.0119	$6e_2' \rightarrow 8e_2'$				
$Ag_6H_6(^1A_{1g})$	247	0.0771	$7e_{1u} \rightarrow 6a_{1g}$	$Au_6H_6(^1A_{1g})$	289	0.2072	$7e_{2g} \rightarrow 5b_{1u}$
	233	0.5357	$7e_{2g} \rightarrow 5b_{1u}$		254	0.0068	$2b_{2g} \rightarrow 5b_{1u}$
	210	0.1873	$5a_{1g} \rightarrow 3a_{2u}$		249	0.0003	$6e_{2g} \rightarrow 5b_{1u}$

[a] Only transitions with oscillator strengths stronger than 0.001 are considered.

Scheme 4

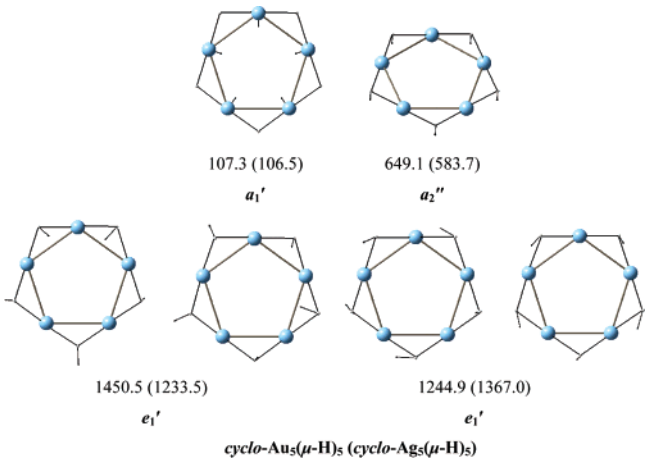

Scheme 5

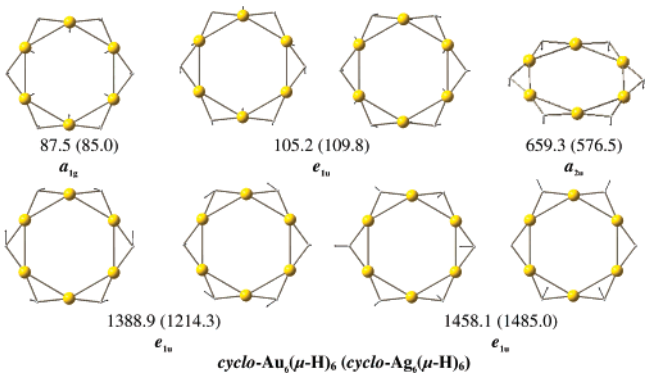

and 707 cm^{-1}, respectively, corresponds to the symmetric out-of-plane vibration of the bridging hydride ligands. Finally, the vibrations related with the symmetric (a_{1g}) and asymmetric (e_u) breathing modes of the M_4 squares absorb in the region 132−138 cm^{-1}, with the former being only Raman active.

For *cyclo*-$Ag_5(\mu\text{-H})_5$ and *cyclo*-$Au_5(\mu\text{-H})_5$ (Scheme 4), the more-intense vibrational modes of e_1' symmetry absorbing at about 1367 and 1245 cm^{-1} respectively are attributed to the asymmetric vibrations of the bridging hydride ligands around the M_5 pentagons. The next-intense vibrational modes of e_1' symmetry, absorbing at 1234 and 1451 cm^{-1}, respectively, correspond to the asymmetric vibrations of the bridging hydride ligands toward the M_5 pentagons. The a_2'' vibration at 584 and 649 cm^{-1}, respectively is assigned to the symmetric out of plane vibration of the bridging hydride ligands. Moreover, the vibrations related to the symmetric (a_1') and asymmetric (e_2') breathing modes of the M_5 pentagons absorb in the region 132−138 cm^{-1}, with the former being only Raman active.

Finally, for the *cyclo*-$Ag_6(\mu\text{-H})_6$ and *cyclo*-$Au_6(\mu\text{-H})_6$ (Scheme 5), the more-intense vibrational modes of e_1' symmetry, absorbing at about 1485 and 1458 cm^{-1}, respectively, are attributed to the asymmetric vibrations of the bridging hydride ligands toward the M_6 hexagons. The next-intense vibrational modes of e_{1u} symmetry, absorbing at 1214 and 1389 cm^{-1}, respectively, correspond to the asymmetric vibrations of the bridging hydride ligands around the M_6 hexagons. The a_{2u} vibration at 577 and 659 cm^{-1}, respectively, is assigned to the symmetric out-of-plane vibration of the bridging hydride ligands. The vibrational modes related with the symmetric (a_{1g}) and asymmetric (b_{1u} and e_{2g}) breathing modes of the M_6 hexagons absorb in the region 34−88 cm^{-1}, with all of them being only Raman active.

In summary, the vibrational modes of the cyclic hydrosilvers(I) and hydrogolds(I) resemble those of the aromatic hydrocarbon analogues, and the corresponding infrared absorption bands could assist in identifying the respective cyclic hydrometals.

Electronic Spectra of the Cyclic Hydrosilvers(I) and Hydrogolds(I). The principal singlet−singlet electronic transitions, excitation energies, and oscillator strengths of the Ag_nH_n (n= 3−6) and Au_nH_n ($n = 3-6$) molecules calculated with the TD-DFT using the B3LYP functionals are given in Table 7.

It can be seen that all excitations occur in the ultraviolet region of the spectra. For all compounds, except $Ag_3(\mu\text{-H})_3$, we obtained three to four dipole-allowed transitions, respectively, that represent the possible absorptions of the compounds. For *cyclo*-$Ag_3(\mu\text{-H})_3$, the number of dipole-allowed transitions obtained was six. All transitions showed a red-shift in hydrogolds(I) with respect to hydrosilvers(I), probably as a result of the aurophilic interactions being stronger than the argentophilic interactions.

The bands with the higher intensity in the *cyclo*-$Ag_n(\mu\text{-H})_n$ ($n = 3-6$) compounds occur at 237, 236, 228, and 233 nm for

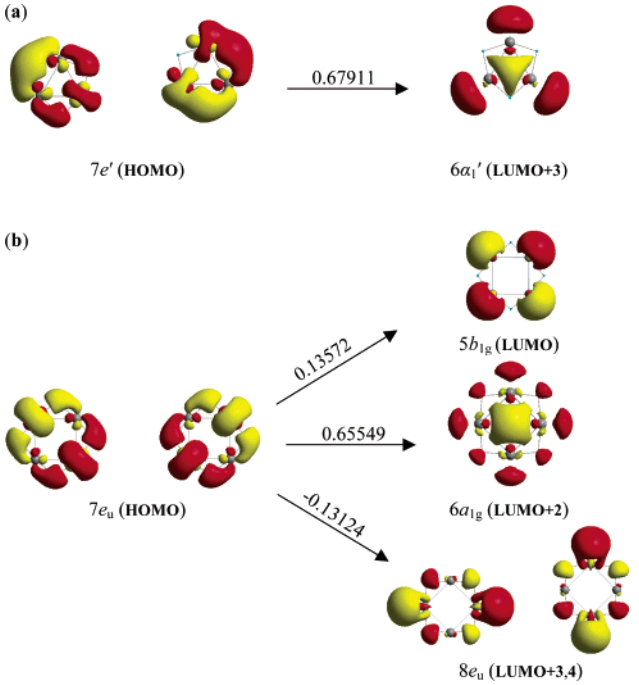

Figure 5. Single-electron transitions with the CI coefficients in the TD-DFT calculations for the more-intense bands of the *cyclo*-Ag_3H_3 (a) and *cyclo*-Ag_4H_4 (b).

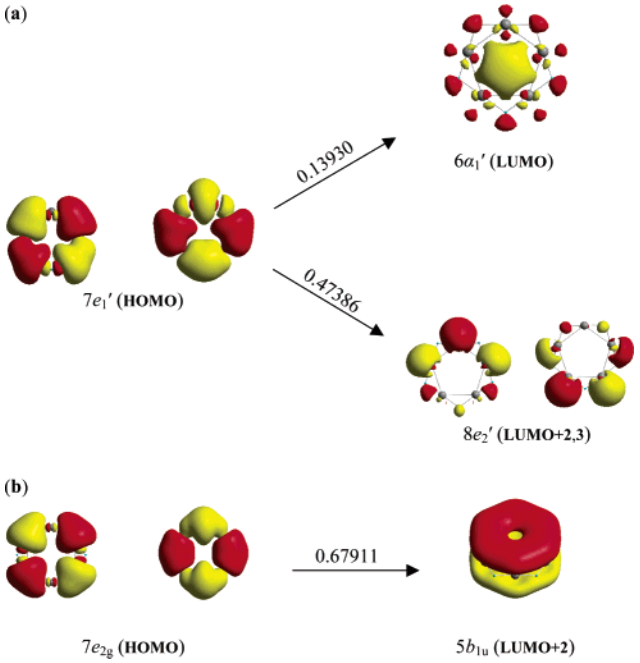

Figure 6. Single-electron transitions with the CI coefficients in the TD-DFT calculations for the more-intense bands of the *cyclo*-Ag_5H_5 (a) and *cyclo*-Ag_6H_6 (b).

the three-, four-, five- and six-membered ring systems, respectively. These bands arise from the electronic transitions from the HOMO to LUMO+2 in the four-, five- and six-membered metallic rings and to LUMO+3 in the three-membered metallic ring. In some cases, some other excited configurations are also mixed with the main excited configuration, having the largest coefficient in the CI wave functions. To intuitively understand the absorption processes, the density diagrams of the participating MOs are depicted in Figures 5 and 6.

It can be seen that these bands are σ^*(Ag−H) → Ag(sp)$_\sigma$ charge-transfer (CT) bands. The lower-energy absorption bands of the *cyclo*-Ag_nH_n (n = 3−6) compounds occur at 292, 273, 246, and 247 nm for the three-, four-, five-, and six-membered metallic rings, respectively. These absorption bands arising from the HOMO → LUMO excitations also correspond to σ^*(Ag−H) → Ag(sp)$_\sigma$ CT bands. On the other hand, the higher-energy absorption bands of the *cyclo*-Ag_nH_n (n = 3−6) compounds occurring at 210, 201, 218, and 210 nm for the three-, four-, five-, and six-membered metallic rings, respectively, correspond to Ag(d)$_{\sigma^*}$ → Ag(sp)$_\sigma$ or Ag(d)$_\pi$ → Ag(p)$_\pi$ metal-centered charge-transfer (MCCT) transitions. Notice that the $Ag_3(NHC)_3$ complex[19] exhibits absorption bands in the ultraviolet region of the electronic spectra at 240−260 nm, with a tail at 300 nm, in line with the predicted absorption bands for the *cyclo*-Ag_3H_3 compound. Similarly, the tetranuclear $[Ag_4]^{4+}$ cluster, stabilized by an *N*-heterocyclic carbene macrocycle,[22] absorbs in the ultraviolet region at 261 and 232 nm, which is also in excellent agreement with the predicted absorption bands for the *cyclo*-Ag_4H_4 compound.

The *cyclo*-Au_nH_n (n = 3−6) compounds exhibit a similar pattern of absorption spectra to that of the *cyclo*-Ag_nH_n (n = 3−6) ones. The most salient feature of the spectra is that, in all transitions, the excitations involve the LUMO of the clusters. Thus, the absorption bands with the higher intensity are the lower-energy bands at 324, 356, 264, and 289 nm for the three-, four-, five-, and six-membered metallic rings, respectively. In these bands, the transitions arise from the HOMO → LUMO excitations, with their nature corresponding to σ^*(Au−H) → Au(sp)$_\sigma$ CT bands. On the other hand, the higher-energy absorption bands of the *cyclo*-Au_nH_n (n = 3−6) compounds occurring at 254, 287, 239, and 249 nm for the three-, four-, five-, and six-membered metallic rings, respectively, correspond mainly to Au(d)$_{\sigma^*}$ → Au(sp)$_\sigma$ MCCT transitions. Finally, the absorption band of *cyclo*-Au_3H_3 with the highest intensity is a σ^*(Au−H) → Au(sp)$_\sigma$ CT band occurring at 237 nm. Noteworthy is the excellent agreement of the predicted excitation energies of the electronic transitions of the *cyclo*-Au_nH_n (n = 3−6) compounds with those of analogous Au(I) polynuclear compounds obtained experimentally.[29b,32b,34,45] Thus, the excitation spectrum of the triangular $Au_3(PhCH_2N{=}COMe)_3$ complex[29b] shows a maximum at 306 nm and a shoulder at 255 nm. The triangular $[(\mu\text{-bpmp})\{Au(C_6F_5)_3\}_3]$ and $[Au_3(\mu\text{-bpmp})_2](CF_3SO_3)_2$ compounds absorb at about 310 and 350 nm, respectively, while the tetranuclear compound is between the two cases.[45] Similarly, the tetranuclear $[Au_4(ArNC(H)NAr)_4]$ complex involving a square planar Au_4 core[32b] absorbs at 260 and 375 nm, while the $[Au_4(\mu\text{-3,5-}^tBu_2\text{-pz})_4]$ compounds exhibits a strong absorption band at 230 nm.[34]

Vertical Electron Detachment Energies (VDEs) of the Cyclic Hdrosilvers(I) and Hydrogolds(I). In Table 8**,** we present results of our calculations of the four lowest-lying vertical one-electron detachment processes from the ground of the *cyclo*-Ag_nH_n and *cyclo*-Au_nH_n (n = 3−6) molecules.

The lowest-energy peak expected to be observed in the photoelectron spectra of all hydrometals(I), according to our calculations, involves detachment of an electron from the doubly occupied HOMO and produces the respective cationic species [*cyclo*-M_nH_n]$^+$ (M = Ag or Au; n = 3−6). The next three peaks, A, B, and C, involve detachment of an electron from the doubly

Table 8. Vertical Electron Detachment Energies and Pole Strengths of the *cyclo*-Ag_nH_n and *cyclo*-Au_nH_n ($n = 3-6$) Molecules Computed with the outer Valence Green's Function (OVGF) Method Using the LANL2DZ Basis Set

compound	*VDE* (eV)	pole strength	Koopmans theorem (eV)	detachment channel
Ag_3H_3 (Au_3H_3) ($^1A_1'$)	8.07 (9.06)	0.925 (0.909)	9.18 (10.14)	$7e'$ ($7e'$)
	9.81 (9.93)	0.918 (0.896)	11.09 (11.42)	$5\alpha_1'$($7\alpha'$)
	9.54 (9.83)	0.875 (0.862)	13.43 (13.33)	$2\alpha_2'$ ($3e''$)
	10.10 (9.70)	0.878 (0.861)	13.90 (13.33)	$3e''$ ($6e'$)
Ag_4H_4 (Au_4H_4) ($^1A_{1g}$)	8.50 (8.38)	0.920 (0.902)	9.83 (10.11)	$7e_u$ ($7e_u$)
	9.38 (10.15)	0.927 (0.918)	10.23 (11.14)	$3b_{2g}$ ($2a_{2g}$)
	9.70 (9.87)	0.918 (0.892)	11.03 (11.84)	$5a_{1g}$ ($5a_{1g}$)
	9.53 (8.44)	0.872 (0.869)	13.49 (11.89)	$2a_{2g}$ ($2b_{2u}$)
Ag_5H_5 (Au_5H_5) ($^1A_1'$)	8.79 (8.91)	0.920 (0.899)	10.15 (10.69)	$7e_1'$ ($7e_1'$)
	9.25 (8.99)	0.924 (0.902)	10.32 (10.73)	$7e_2'$ ($7e_2'$)
	9.49 (9.87)	0.920 (0.896)	10.81 (11.69)	$5\alpha_1'$ ($2a_2'$)
	9.67 (8.57)	0.872 (0.870)	13.63 (11.99)	$2a_2'$ ($1a_1''$)
Ag_6H_6 (Au_6H_6) ($^1A_{1g}$)	8.98 (8.83)	0.922 (0.901)	10.23 (10.61)	$7e_{2g}$ ($7e_{2g}$)
	8.93 (9.21)	0.921 (0.899)	10.30 (10.98)	$7e_{1u}$ ($7e_{1u}$)
	9.30 (9.77)	0.921 (0.899)	10.63 (11.51)	$3b_{2u}$ ($4b_{1u}$)
	9.79 (10.43)	0.928 (0.918)	10.62 (11.49)	$5a_{1g}$ ($2a_{2g}$)

Scheme 6

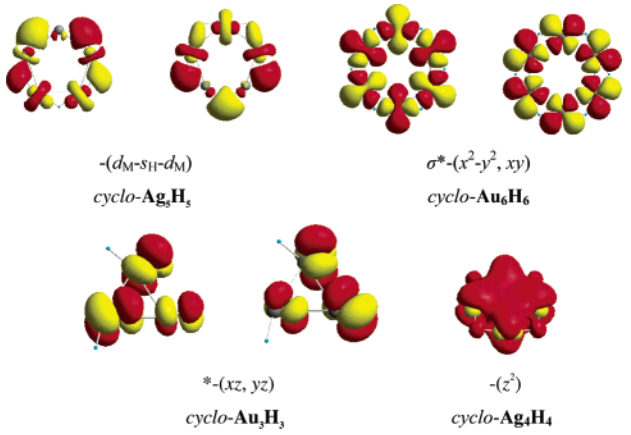

occupied σ-(d_M-s_H-d_M) MOs localized on the M−H−M skeletons, the σ^*-(x^2-y^2, xy) MOs, the π^*-(xz, yz) MOs, and the δ-(z^2) MOs delocalized over the metallic skeleton of the rings. A few representative MOs participating in the electron detachment processes are shown in Scheme 6.

It is important to compare the computed VDEs of the hydrosilvers(I) and hydrogolds(I) to those of the benzene molecule; the X, A, B, and C peaks of benzene were predicted to occur at 8.65, 8.67, 11.21, and 11.30 eV, respectively, with second-order pole strengths in the range of 0.876−0.888. The excellent agreement of the VDEs of the hydrosilvers(I) and hydrogolds(I) to those of the benzene molecule strongly suggests that the all-metal Ag(I) and Au(I) rings possess the characteristic feature of aromaticity inherent to the aromatic hydrocarbons.

Interaction of the *cyclo*-$Au_6(\mu$-H)$_6$ Molecule with Ag^+ Ions. To verify further the aromaticity of the hydrosilvers(I) and hydrogolds(I), we also used a chemical reactivity criterion of aromaticity, that of the interaction of the aromatic molecules with electrophiles. In particular, we studied the reaction of *cyclo*-$Au_6(\mu$-H)$_6$ molecule with Ag^+ ions, based on a very recent investigation of a stable $[Au_6Ag\{\mu$-$C_6H_2(CHMe_2)_3\}_6]^+$ complex which looks like an Au_6Ag wheel with a gold rim.[51] Actually, in this complex, a silver(I) atom was incorporated into the center of a perfect Au_6 hexagon. Searching the potential energy surface (PES) of the $[Ag\{$*cyclo*-$Au_6(\mu$-H)$_6\}]^+$ system, we found a global minimum corresponding to a hexagonal pyramid with C_{6v} symmetry, and very close to the global minimum, we located a transition state only 0.9 kcal/mol higher in energy, corresponding to a perfect hexagon with D_{6h} symmetry, incorporating at its center the Ag(I) ion. The equilibrium structures of the ground and the transition state of the $[Ag\{$*cyclo*-$Au_6(\mu$-H)$_6\}]^+$ cluster are depicted schematically in Figure 7.

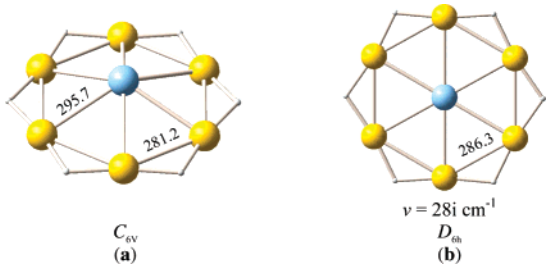

Figure 7. Equilibrium geometries of the global minimum (a) and the transition state (b) of the $[Ag\{$*cyclo*-$Au_6(\mu$-H)$_6\}]^+$ cluster computed at the B3LYP level of theory using the LANL2DZ basis set for Ag atoms, the LANL2DZ basis set plus an f polarization function ($\alpha_f = 0.75$) for Au atoms, and the cc-pVQZ basis set for H atoms.

It can be seen that the Au_6 skeleton in both the ground and the transition state correspond to perfect hexagons with all six Au−Au bond distances equivalent (281.2 pm for the C_{6v} structure and 286.3 pm for the D_{6h} one) and Au−Au−Au bond angles of 60.0°, while the Au−Ag bond distances, also being equivalent, are 295.7 and 286.3 pm for the C_{6v} and D_{6h} structures, respectively, and the Au−Ag−Au bond angles are 60.0° as well. In the C_{6v} structure, the Ag(I) ion is displaced along the C_6 axis over the hexagonal basal plane by 91.8 pm. It is important to be noted that, despite the different bridging ligands, the structure of the $[Ag\{$*cyclo*-$Au_6(\mu$-H)$_6\}]^+$ cluster closely resembles that of the experimental $[Au_6Ag\{\mu$-C_6H_2-$(CHMe_2)_3\}_6]^+$ cluster. In the latter, the Au−Au bond distances range from 279.5 to 281.7, the Ag−Au bond distances range from 279.7 to 280.9 pm, and the Au−Ag−Au bond angles are almost equal to 60.0°. The Ag(I) ion is found at the center of the plane defined by the Au_6 core.[51] This position of the Ag(I) should be the vibrationally averaged position for an Ag(I) ion oscillating with respect to the Au_6 plane. Notice that this umbrella-like inversion process, involving a planar transition state of D_{6h} symmetry, is a barrierless process; the computed activation barrier is less than 1 kcal/mol. The imaginary

Scheme 7

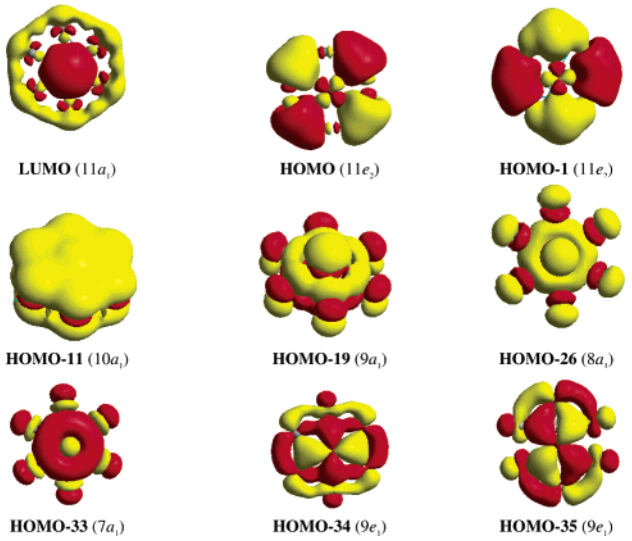

frequency at 28*i* cm^{-1} corresponds to the oscillation of the Ag(I) ion with respect to the inversion center of the six-membered gold(I) ring.

To get insight into the bonding mechanism of the Ag^+ ion with the *cyclo*-$Au_6(\mu\text{-}H)_6$ molecule, we went carefully through the valence MOs of the cluster, and the most relevant ones are shown in Scheme 7.

It can be seen that the bonding of the central Ag(I) ion with the six-membered gold(I) ring involves covalent σ, π, and δ components as it is exemplified by the highly delocalized σ -, π-, and δ-type MOs, which support a charge transfer from the six Au(I) atoms toward the Ag(I) central atom, the latter acquiring a positive natural charge of 0.56 charge units. This charge transfer is also mirrored on the deshielding of the Au(I) atoms, which showed a downfield shift of the ^{197}Au shielding tensor element by 15.7 ppm. Moreover, the computed interaction energy between the Ag(I) ion and the aromatic six-membered gold(I) ring was found to be 52.1 kcal/mol and corresponds to 8.7 kcal/mol per Ag−Au bond formed, a value lying in the range of the so-called aurophilic interaction energy.

The most-characteristic infrared-active vibrational modes of the $[Ag\{cyclo\text{-}Au_6(\mu\text{-}H)_6\}]^+$ cluster along with the normal coordinate vectors (arrows) which could help experimentalists in identifying such clusters are shown in Scheme 8.

Finally, the principal singlet−singlet electronic transitions, excitation energies, and oscillator strengths of the $[Ag\{cyclo\text{-}Au_6(\mu\text{-}H)_6\}]^+$ cluster calculated with the TD-DFT using the B3LYP functionals resemble those of the precursor *cyclo*-$Au_6(\mu\text{-}H)_6$ molecule. Thus, the dipole-allowed transitions of higher intensity absorb at 274, 297, and 315 nm with oscillator strengths of 0.0894, 0.2624, and 0.0052 and are assigned to $10e_1 \rightarrow 11a_1$, $11e_2 \rightarrow 7b_1$, and $11e_2 \rightarrow 11a_1$ electronic transitions, respectively. All electronic transitions correspond to charge transfer from the Au_6 metallic ring to the central Ag(I) ion.

Concluding Remarks

In this paper, we have reported a comprehensive DFT study of the structural, energetic, spectroscopic (IR, NMR, UV−vis, and photoelectron), electronic, and bonding properties of a new series of hydrosilver(I) and hydrogold(I) analogues of aromatic hydrocarbons. These novel classes of inorganic compounds can be considered as the archetypes for the development of whole classes of new inorganic aromatic species (substituted derivatives), resulting upon substitution of the H atoms by other groups, such as alkyls (R) and aryls (Ar), halides (X), amido (NR_2), hydroxide (OH) and alkoxides (OR), etc.

The results can be summarized as follows.

All *cyclo*-Ag_nH_n and *cyclo*-Au_nH_n ($n = 3-6$) molecules have a structure analogous to the corresponding aromatic hydrocarbons, which is characterized by perfect planarity and equalization of all metal−metal bonds in the aromatic metallic rings. Novel low-energy 3D structures of the Ag_nH_n and Au_nH_n ($n = 3-6$) molecules were also identified as local minima in the potential energy surfaces, but at 34−59 kcal/mol higher in energy than the 2D planar ones. The planar hydrosilvers(I) and hydrogolds(I) are predicted to be strongly bound molecules with respect to their dissociation either to the MH monomers or to free M and H atoms in their ground states. The computed total binding energies of the MH monomers to form the *cyclo*-M_nH_n species are found in the range of 7.5−188.5 kcal mol^{-1}. On the other hand, the computed binding energies per mole of the monomers MH ranging from 19.5 to 31.4 kcal/mol accounts for the sum of the M−M and M−H−M bond energies. Moreover, the formation of the *cyclo*-M_nH_n species from the standard states of their elements, M(s) and H_2(g) correspond to exothermic processes with predicted exothermicities in the range of −59.1 to −265.3 kcal/mol.

On the basis of the predicted stability of the hydrosilvers(I) and hydrogolds(I) with respect either to the constituent atoms or to the standard states of their elements, one would expect both the neutral and cationic species to be formed in MS of gold vapor sputtered with hydrogen or by the normal spectroscopic approach of deposition of the metal in a hydrogen matrix. Moreover, the hydrosilvers(I) and hydrogolds(I) could be synthesized even by appropriate chemical processes analogous to those used for the synthesis of the M_nR_n (M = Cu, Ag, Au; R = alkyl or aryl) derivatives.

The bonding of all *cyclo*-$M_n(\mu\text{-}H)_n$ species is characterized by a common ring-shaped electron density, more commonly seen in organic molecules, which is constructed by highly delocalized σ-, π-, and δ-type MOs.

We have also reported the computed spectroscopic properties (IR, NMR, UV−vis, and photoelectron) of hydrosilvers(I) and hydrogolds(I) in order to assist in identifying the respective aromatic hydrometals(I) and help for future laboratory studies. A complete assignment of the most-characteristic infrared absorption bands is given, while the aromaticity of the hydrometals(I) was estimated by making use of several criteria for aromaticity, such as the NICS(0) parameter, the relative hard-

Scheme 8

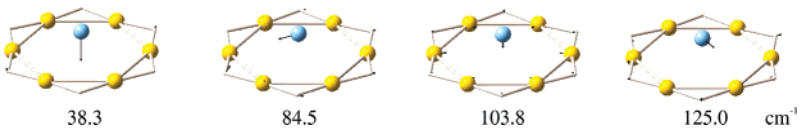

ness, $\Delta\eta$, and the electrophilicity index, ω. The principal singlet−singlet electronic transitions, excitation energies, and oscillator strengths of the aromatic hydrosilvers(I) and hydrogolds(I) were calculated with the TD-DFT using the B3LYP functionals and the complete assignment of the electronic transitions is given. Moreover, the VDEs from the neutral hydrosilvers(I) and hydrogolds(I) were computed with the OVGF method to help experiment in assigning the features of the photoelectron spectra of the compounds.

Finally, the aromaticity of hydrosilvers(I) and hydrogolds(I) was further verified on the grounds of a chemical reactivity criterion of aromaticity, that of the interaction of the aromatics with electrophiles, presenting only one example concerning the reaction of *cyclo*-$Au_6(\mu\text{-}H)_6$ molecule with Ag^+ ions. Actually, this interaction affords the $[Ag\{cyclo\text{-}Au_6(\mu\text{-}H)_6\}]^+$ species, which adopts an hexagonal pyramidal structure of C_{6v} symmetry with the silver(I) ion displaced along the C_6 axis over the hexagonal basal plane by 91.8 pm.

Supporting Information Available: The harmonic vibrational frequencies and the IR intensities in Table S1 and the Cartesian coordinates and energies of all stationary points compiled in Tables S2 and S3, respectively. This material is available free of charge via the Internet at http://pubs.acs.org.

JA0469277